

**Report 95.040**

**NAS-94 Interpretation Report  
Part III: Combined interpretation  
of aeromagnetic and gravity data**

Report no. 95.040		ISSN 0800-3416		Grading: Confidential to 2000	
Title: NAS-94 Interpretation Report Part III: Combined interpretation of aeromagnetic and gravity data					
Author: Odleiv Olesen and Mark A. Smethurst			Client: Mobil Exploration Norway, Norsk Hydro, Statoil and NGU		
County: Nordland and Nord-Trøndelag			Commune:		
Map-sheet name (M=1:250.000) Bodø, Mo i Rana, Vega and Namsos			Map-sheet no. and name (M=1:50.000)		
Deposit name and grid-reference:			Number of pages: 50		Price:
			Map enclosures: 10		
Fieldwork carried out: April-June 1994	Date of report: 29.03.95	Project no.: 61.2543.44	Person responsible: <i>Tor S. Rønnevig</i>		
<p>Summary:</p> <p>A combined interpretation of new aeromagnetic data (NAS-94), existing offshore and onland gravity and new petrophysical data between 64°30' and 68°N is reported. Data from the Nordland Aeromagnetic Survey (NAS-94) has revealed several sets of high frequency anomalies caused by magnetic sources within the sedimentary sequences. When compared with petrophysical measurements on cores from the shallow drilling programme of IKU Petroleum Research, the anomaly pattern is interpreted to represent three types of sources; 1) Quaternary overburden of varying thickness and bathymetric features, 2) buried magnetic sedimentary rocks, sub-cropping sedimentary units and possible magnetic fault zones, 3) magnetic basement in the Lofoten Horst, Nordland Ridge, south central part of the Trøndelag Platform and mainland Norway.</p> <p>The sub-cropping wedge of Permian to Tertiary sediments along the inner Trøndelag Platform causes a distinct set of sub-parallel anomalies. A correlation between anomalies caused by early Cretaceous faulting on the Vega High and anomalies due to underlying basement topography indicates that the deep structural setting may have guided the location of later faulting. Our combined interpretation of magnetic and gravity data sets indicates that a splay of the Ylvingen Fault on the Vega High continues into Ranafjorden on the mainland.</p> <p>Estimates of depths to basement from gravity data are generally shallower than estimates from magnetic data in the same area. For example, interpretation of depths to basement from gravity and aeromagnetic data gives depths of 6 - 8 km and 8 - 12 km respectively for the central part of the Helgeland Basin. This phenomenon may be due to 1) the presence of low-magnetic basement rocks beneath the basin (comparable to the Helgeland or Rødingsfjell Nappe Complexes on the mainland) or 2) a low density contrast between the sediments and the underlying crystalline basement. The former explanation seems to be the case for the Rødøy High along the Nordland Ridge where depths to magnetic basement exceed basement depths obtained from exploration drilling. The combined interpretation of depths to basement from gravity and aeromagnetic data reveals a complex system of fault blocks along the Nordland Ridge. Depths to the basement in the Træna Sub-basin are in the range 9-12 km and in the outer part of the Vestfjorden Basin between 7 and 8 km.</p>					
Keywords: Geofysikk		Kontinentalsokkel		Tolkning	
Berggrunnsgeologi		Magnetometri		Forkastning	
Petrofysikk		Gravimetri		Fagrapport	

## CONTENTS

1 INTRODUCTION.....	4
2 MAIN STRUCTURAL ELEMENTS WITHIN THE SURVEY AREA .....	5
3 DATA SETS.....	6
3.1 Aeromagnetic data.....	6
3.2 Gravity data .....	6
3.3 Petrophysical data.....	7
3.4 Bathymetric and topographic data .....	11
4 PROCESSING AND INTERPRETATION METHODS .....	12
4.1 Map production and data enhancement .....	12
4.2 Determination of depth to anomaly sources.....	13
4.3 Forward modelling.....	15
4.4 Geophysical interpretation map.....	16
5 INTERPRETATION AND DISCUSSION.....	17
5.1 General aeromagnetic and gravity features .....	17
5.2 Depth to basement .....	18
5.3 High frequency aeromagnetic anomalies.....	19
6 CONCLUSIONS .....	21
7 ACKNOWLEDGEMENTS .....	23
8 REFERENCES .....	23
List of figures and maps .....	26

## 1 INTRODUCTION

The Nordland Aeromagnetic Survey is a collaboration project between Mobil Exploration Norway, Norsk Hydro, Statoil and the Geological Survey of Norway (NGU). During the period April to June 1994 NGU conducted an aeromagnetic survey offshore Nordland from 64° 30' to 68°N covering parts of the Nordland I-VI areas (Fig. 1). The survey area extends from the Træna Sub-basin to the west and eastward to the coast of Nordland and covers consequently the northernmost part of the Trøndelag Platform including the main structural elements Nordland Ridge, Helgeland Basin, Vega High and parts of Vestfjorden Basin and Træna Sub-basin. A combined interpretation of this data-set with gravity and petrophysical data from both the offshore and mainland areas was carried out. The offshore petrophysical data consist of susceptibility measurements on cores from IKUs shallow drilling programme.

The project was consequently organised within three sub-projects:

I) Interpretation of aeromagnetic data

II) Measurements of petrophysical data

III) Combined interpretation of aeromagnetic, gravity and petrophysical data

The present report covers sub-project III the combined interpretation of aeromagnetic, gravity and petrophysical data. The results of the two other sub-projects were presented in NGU Reports 94.074 and 95.039 (Olesen & Smethurst 1994 and Mørk & Olesen 1995, respectively).

## 2 MAIN STRUCTURAL ELEMENTS WITHIN THE SURVEY AREA

Fig. 1 shows the main structural elements within the bedrock offshore Nordland (Blystad et al. in prep.). The bulk of the Nordland Aeromagnetic Survey 1994 survey covers the northern Trøndelag Platform including the Helgeland Basin and the Vega High (Bøen et al. 1984, Gabrielsen et al. 1984, Brekke & Riis 1987, Blystad et al. in press.). The western section of the NAS-94 survey comprises the Nordland Ridge and the eastern part of the Træna Sub-basin within the Vøring Basin. The transition zone between the ridge and the basin consists of a complex zone of fault blocks within the Revfallet Fault Complex. The throws of the faults are in the order of several kilometres. The Lofoten Horst and the Vestfjorden Basin are situated in the northern part of the NAS-94 area. The Rana Fault Complex constitutes the eastern margin of the Trøndelag Platform (Gabrielsen et al. 1984, Bukovics & Ziegler 1985). The Early Cretaceous Vega High (Gabrielsen et al. 1984) is situated within the Trøndelag Platform, and is bounded by the Ylvingen Fault Zone which also defines the southeastern boundary of the Helgeland Basin. Several smaller grabens are situated along the Ylvingen Fault Zone.

At the base Cretaceous level the Trøndelag Platform corresponds to a seaward dipping, relatively little faulted monocline, which grades northward into the gently synformal Helgeland basin. The Trøndelag Platform is underlain by thick Upper Palaeozoic and Triassic strata. Palaeozoic sediments reach their greatest thickness in the east, suggesting a westward shift of the depocentre during Permian and Triassic time (Bukovics & Ziegler 1985).

The basement on the mainland adjacent to the survey area is covered by five 1:250.000 scale bedrock maps; Bodø (Gustavson & Blystad in press), Mo i Rana (Gustavson & Gjelle 1991), Vega (Gustavson & Bugge in press), Mosjøen (Gustavson 1981) and Namsos (Solli et al. in press) and consists mainly of three Precambrian basement terrains and two Caledonian nappe complexes. The Lofoten-Vesterålen area, Høgtuva-Sjona tectonic windows and the Western Gneiss Region make up the Precambrian basement terrains to the north, in the centre and to the south, respectively. The Rødingsfjell and Helgeland Nappe Complexes are situated to the north and south of the Høgtuva-Sjona Tectonic Windows. The Bindal Batholith is situated within the Helgeland Nappe Complex.

### **3 DATA SETS**

#### **3.1 Aeromagnetic data**

The survey was flown with a line spacing of 2 km and a tie-line separation of 5 km (Fig. 2). In all, 36,000 km were flown covering an area of approximately 50,000 km<sup>2</sup>. The flight altitude was 200 metres and the towed bird was located 50 metres below the Piper Chieftain aircraft (i.e. 150 m above sea level). A Scintrex Cesium Vapour MAC-3 magnetometer with a CS-2 sensor was used in the data acquisition. The noise envelope of the towed magnetometer was less than 0.2 nT. Real time differential GPS navigation with a minimum of 4 satellites was used throughout the survey resulting in a navigation accuracy better than  $\pm 10$  m. A more detailed description of the survey is reported by Olesen & Smethurst (1994). The geophysical consultancy company Amarok a.s carried out the processing of the data-set. The processing report is enclosed as an Appendix in the initial interpretation report by Olesen & Smethurst (1994).

#### **3.2 Gravity data**

The present study is based on measurements from 3228 gravity stations on land collected by NGU and the Norwegian Mapping Authority and approximately 25,000 km of marine gravity profiles (Fig. 3) collected by the Norwegian Petroleum Directorate, various oil companies and the Norwegian Mapping Authority. The marine data-sets were compiled and levelled by Amarok a.s. The complete Bouguer reduction (Mathisen 1976) of the gravity data was computed using a rock density of 2670 kg/m<sup>3</sup> on land. The simple Bouguer correction at sea was carried out using a density of 2300 kg/m<sup>3</sup>. The International Standardisation Net 1971 (I.G.S.N. 71) and the Gravity Formula 1980 for normal gravity were used to level the surveys. Two combinations of data-sets; 1) Free air at sea and Bouguer on land and 2) Bouguer at sea and Bouguer on land, were interpolated to square grids of 2 km x 2 km using the minimum curvature method (Swain 1976, Geosoft 1994a). The final grids were moderately smoothed through the application of an upward continuation of 1000 m. Free air and Bouguer anomaly maps at the scale of 1:500,000 (Maps 6 & 7, Figs. 11 & 12) were produced from this grid using the map production system by Geosoft (1994a). Maps 7 and 8 (Figs. 13 & 14) show the residual gravity maps. The separation of residual field is carried out in the frequency domain using 50 and 100 km Gaussian filters (Maps 7 & 8, Figs. 13 & 14). The locations of the gravity stations are shown on the maps.

### 3.3 Petrophysical data

A total of 1659 susceptibility measurements were carried out on cores from the IKU shallow drilling programme [seasons 1982 (southern Helgeland), 1991 (Lofoten) and 1992 (northern Helgeland)]. This petrophysical study was reported separately as Part II of the NAS-94 interpretation report (Mørk & Olesen 1995). The frequency distribution of susceptibilities for the most common rock units are presented by Olesen & Smethurst (1994) and Mørk & Olesen (1995). The distributions are generally wide, covering one or two orders of magnitude. Sandstone has a lower susceptibility than mudstone, siltstone and claystone,  $50\text{-}300 \times 10^{-6}$  SI versus  $150\text{-}600 \times 10^{-6}$  SI. This is comparable with the susceptibility of the metamorphosed paramagnetic equivalents on land in Norway (e.g. histograms from Rødingsfjell and Helgeland Nappe Complexes). Ferro-magnetic meta-sediments in the crystalline basement on the mainland may, however, have more than two orders of magnitude higher susceptibility than the paramagnetic equivalents. Red-coloured sandstones often have higher susceptibilities than other kinds of sediments within the NAS-94 area, up to  $1000 \times 10^{-6}$  SI. The highest susceptibility recorded in bedrock lithologies was encountered in siderite cemented clay- and silt-stones of Cretaceous age; up to  $4000 \times 10^{-6}$  SI. These cemented zones occur in 5-20 cm wide sections in the IKU cores and seem locally to be associated with small-scale faulting. Caliche which is a lithified desert soil formed by the near surface crystallisation of calcite and/or other soluble minerals by upward-moving solutions, has intermediate susceptibilities reaching  $1000 \times 10^{-6}$  SI. The study of the minerals causing increased susceptibilities will be reported in the interpretation report Part II. Gypsum and coal have the lowest susceptibilities, the former has susceptibilities in the range  $-20$  to  $+10 \times 10^{-6}$  SI, i.e. gypsum can be diamagnetic – a finding consistent with published data (e.g. Telford et al. 1976).

The Quaternary overburden, especially glaciomarine clay, has even higher susceptibilities than the underlying sedimentary rocks. The source of the Quaternary sediments are in part very magnetic crystalline basement rocks on mainland Norway. The values vary between 60 and  $6000 \times 10^{-6}$  SI.

As constraints for the gravity modelling we have used information from petroleum exploration wells on the Nordland Ridge and the Utgard High. The densities of sedimentary sequences calculated from density logs are shown in Table 2. These estimates were used to constrain 2½D modelling along profiles TB-38-87, PROFILE D and PROFILE E (Map 5, Fig. 11).

Table 1. Statistical data; (A) density, susceptibility and Q-value for the main rock-units in IKU's shallow drill cores, (B) density, susceptibility and Q-value of hand specimens from the Caledonides and Precambrian rocks of Nordland and North-Trøndelag (Mørk & Olesen 1995). Sample locations are shown in Fig. 5. The letters a, b and c denote total sample, low-magnetic fraction and high-magnetic fraction, respectively. SI units are used.

**A) OFFSHORE DRILL CORES**

ROCK UNIT/TYPE	No.	SUSCEPTIBILITY			
		min	max	mean	std
PLEISTOCENE	55	0.00006	0.00625	0.00107	0.00151
OLIGOCENE	8	0.00006	0.00081	0.00032	0.00027
PALAEOCENE	5	0.00013	0.00024	0.00019	0.00004
UPPER CRETACEOUS (incl. siderite)	25	0.00010	0.00256	0.00060	0.00071
LOWER CRETACEOUS (incl. siderite)	45	0.00006	0.00320	0.00092	0.00073
UPPER CRETACEOUS (excl. siderite)	14	0.00010	0.00027	0.00017	0.00005
LOWER CRETACEOUS (excl. siderite)	19	0.00019	0.00112	0.00034	0.00022
CRETACEOUS siderite	37	0.00006	0.00320	0.00129	0.00071
UPPER JURASSIC	37	0.00006	0.00159	0.00040	0.00049
MIDDLE JURASSIC	50	0.00001	0.00200	0.00010	0.00028
LOWER JURASSIC	73	0.00001	0.00300	0.00038	0.00049
LOWER TRIASSIC	863	0.00002	0.00143	0.00027	0.00016
UPPER PERMIAN	488-0	0.00008	0.00085	0.00014	0.00013

**B) LAND MEASUREMENTS**

ROCK UNIT/TYPE	No.	DENSITY				No.	min	Q-VALUE			No.	SUSCEPTIBILITY				
		min	max	mean	std			min	max	mean		std	min	max	mean	std
RØDINGSFJELL NAPPE COMPLEX	a	411	2311	3430	2798	142	217	0.00	175.11	3.34	12.91	411	0.00000	6.00000	0.02855	0.30248
	b											351			0.00046	0.00047
	c											60			0.19291	0.77143
HELGELAND NAPPE COMPLEX	a	506	2488	3273	2808	128	497	0.00	251.76	4.13	15.37	506	0.00000	0.67692	0.00461	0.03468
	b											465			0.00056	0.00057
	c											41			0.05058	0.11199
BINDALEN BATHOLITH	a	315	2521	3219	2733	137	315	0.00	161.89	3.85	13.60	315	0.00000	0.14690	0.00358	0.01329
	b											266			0.00048	0.00053
	c											49			0.02040	0.02828
PRECAMB. IN THE LOFOTEN AREA	a	508	2579	3553	2775	135	520	0.00	67.63	1.06	4.05	520	0.00002	4.94550	0.04961	0.22372
	b											142			0.00078	0.00070
	c											378			0.06796	0.26003
SJONA-HØGTUVA TECTONIC WINDOWS	a	1141	2541	2976	2643	39	9	0.00	13.97	3.14	5.53	1141	0.00001	0.14727	0.00839	0.01160
	b											448			0.00082	0.00081
	c											693			0.01329	0.01265
WESTERN GNEISS REG. (Trøndelag)	a	419	2581	3300	2729	106	415	0.02	45.59	1.04	2.76	419	0.00001	0.45812	0.00912	0.02599
	b											241			0.00074	0.00072
	c											178			0.02045	0.03697





Several pronounced magnetic and gravimetric anomalies within the project area are continuous from land onto the continental shelf (Maps 1 & 7, Figs. 6 & 13). It is therefore important to know the densities, susceptibilities and Q-values of the rocks on land when interpreting the potential field data in the offshore area. Approximately 4100 rock samples, collected during geological mapping and geophysical studies were measured with respect to density, susceptibility and remanence. This data-set is presented in detail in the NAS-94 Interpretation report Part II, Petrophysical data (Mørk & Olesen 1995). Statistical data for the main rock units are summarised in Table 1. Q-values, the ratios of remanent to induced magnetisation, are reported rather than NRM intensities. The Q-value was not calculated if the susceptibility is below 0.00150 SI units, since the accuracy of remanence measurements is relatively poor for samples with low induced magnetisation. The sample locations of both hand specimens and offshore cores (IKU's shallow drilling) are shown in Fig. 5 which is a reduced version of the 1:1 million map by Mørk & Olesen (1995).

The frequency distribution of susceptibilities for the most common rock units are shown in the petrophysics report (Mørk & Olesen 1995). The histograms show that the Precambrian rocks (Lofoten-Vesterålen area, Høgtuva-Sjona Tectonic Windows and Western Gneiss Region) are commonly highly magnetic and usually show wide and complex (multimodal) distributions. The high-amplitude magnetic anomalies in the Lofoten archipelago and the Høgtuva-Sjona area are caused by granulite-facies rocks and granites, respectively. Table 1 also shows that Q-values are generally low, in the order of 0.5 or lower. Schlinger (1985) and Olesen et al. (1991) have also shown that the remanence of the rocks in the Lofoten-Vesterålen area is viscous and parallel to the present Earth's field, which make aeromagnetic interpretations in the area simpler. The orthopyroxene isograd in the Vesterålen area coincides with the boundary between the high-magnetic and low-magnetic gneisses. West of this line the migmatites are in granulite-facies metamorphism whereas to the east they have amphibolitic metamorphic grade. The understanding of this isograd is critical for the interpretation of the magnetic field on the mainland as well as on the continental shelf in the Lofoten-Vesterålen area (Schlinger 1985, Olesen et al. 1991). In the Lofoten-Vestfjorden area the magnetic basement surface reflects the depth to the granulite-facies gneisses. We refer the reader to these papers for a detailed discussion of the magnetic properties in the Lofoten - Vesterålen area. The granitic and migmatitic gneisses in the Western Gneiss Region are also often magnetic. A detailed study of the magnetic properties of the rocks in the Roan area located immediately to the south of the NAS-94 area, shows that magnetite is formed during the metamorphic transition from amphibolite- to granulite-facies metamorphism (Skilbrei et al. 1991), analogous to the process occurring in the Lofoten-Vesterålen area.

The average densities for Precambrian basement rocks in the Lofoten-Vesterålen area, the Høgtuva-Sjona windows and Western Gneiss Region (Vestranden) are 2770, 2640 and 2730 kg/m<sup>3</sup>, respectively. The densities of the Rødingsfjell and Helgeland Nappe Complexes (Uppermost Allochthon within the Caledonian Orogen) are 2790 and 2810 kg/m<sup>3</sup> respectively. Samples from the Bindal Batholith which constitutes a significant portion of the Helgeland Nappe Complex, were excluded in the calculation of the density of the nappe complex. The average density of the Bindal

Batholith itself is  $2730 \text{ kg/m}^3$ . The calculated mean density of the basement within the NAS-94 area is  $2750 \text{ kg/m}^3$

### **3.4 Bathymetric and topographic data**

The bathymetric data were provided by the Marine Department of the Norwegian Mapping Authority in Stavanger (care of N.P. Skeie). The data set has three different sources; 1) modern multi-beam echo sounder measurements in the Vestfjorden area, 2) digitised naval maps in areas adjacent to the coast and 3) water depth data collected during seismic surveys. The quality of the data sets varies considerably. Data set 1 has the highest quality while data set 3 is the poorest. The data-set is interpolated onto a regular grid using the minimum curvature method (Swain 1976). The cell size of the combined grid is  $1.5 \text{ km} \times 1.5 \text{ km}$ .

The land topography grid originates from the Norwegian Mapping Authority in Hønefoss. These data were utilised for several years at NGU for terrain correction of gravity measurements. The grid had an original cell size of  $100\text{m} \times 100\text{m}$  but for our purposes was resampled to produce a  $300 \times 300 \text{ m}$  grid. The THEMATIC map production system (Kihle 1992) is applied to produce the bathymetric/topographic map (Map 9 & Fig. 15). The flight pattern diagram of the NAS-94 survey is added to this map.

## 4 PROCESSING AND INTERPRETATION METHODS

### 4.1 Map production and data enhancement

The aeromagnetic, gravity, bathymetric and topographic data were interpolated to regular grids using the minimum curvature method (Swain 1976). The sizes of the grid cells were 500, 2000, 1500 and 300 m, respectively. The US Geological Survey minimum curvature computer algorithm (Cordell et al. 1992) was applied in favour of that supplied by Geosoft (1994a) because of its higher resolution data storage (REAL\*4 compared with INTEGER\*2). We have found that the INTEGER\*2 data storage format is insufficient for data types with extremely high dynamic ranges such as the modern aeromagnetic data from NAS-94 (and the preceding VIKING-93 Project). Residual aeromagnetic data with reduced data ranges can, however, be safely stored in INTEGER formats. The magnetic total field referred to IGRF 1994 displayed at a scale of 1:500,000 in Map 1 and Fig. 6. Maps at a scale of 1:250,000 is presented in Part I of the NAS-94 interpretation report (Olesen & Smethurst 1994).

Enhancement techniques akin to those commonly used in image processing were applied to the geophysical data, along with the more traditional geophysical post-processing enhancements. Histogram-equalisation, high-frequency filtering and shaded-relief presentation were used as standard techniques in the map production. Shaded-relief presentations, which treat the grid as topography illuminated from a particular direction, have the property of enhancing lineaments which lie oblique to the direction of illumination. A map of stacked Hanning filtered profiles (Map 8 of Olesen & Smethurst 1994) was produced to show the shape of individual high frequency anomalies to help in establishing the dip and depth of the sources of the anomalies. The separation of the field into residual and regional components (both gravity and magnetic data) is carried out in the frequency domain using Gaussian filters (Geosoft 1994b) to minimise 'ringing'.

The analytic signal (amplitude of the total magnetic gradient) is displayed in Map 2 and Fig. 7. The horizontal gradient in the north-south direction was generated to enhance a set of very subtle WNW-ESE trending anomalies (Map 3 and Fig. 8). We have in the present report produced a map of the 15 km high-pass Gaussian filtered anomalies (Map 4, Fig. 9). Frequency filtered maps showing anomalies within three different wave length ranges; less than 5 km, 5 - 15 km and longer than 15 km (referred to as depth slices 1, 2 and 3) were supplied by Olesen & Smethurst (1994). The aeromagnetic data were upward continued 200 m before calculating the gradient maps (Map 2 & 3). More details about the gridding and filtering can be found in the initial interpretation report (Olesen & Smethurst 1994). The separation of residual field is carried out in the frequency domain using 50 and 100 km Gaussian filters (Maps 7 & 8, Figs. 13 & 14). The gravity data were upward continued 1000 m before filtering. The map production was carried out with the Geosoft system (Geosoft 1994a) and the THEMATIC system from NGU (Kihle 1992). The depth estimates to anomaly sources (both magnetic and gravimetric) are included on the maps, as are the fault

interpretation of Blystad et al. (in prep.) and the locations (and in one case depths) of exploration wells (up to September 1993).

#### 4.2 Determination of depth to anomaly sources

The autocorrelation method (Phillips 1975, 1979, Torsvik & Olesen 1992) was used to estimate the depth to the basement from aeromagnetic profile data. The magnetic basement is defined as a two-dimensional surface constructed from a large number of very thin vertical 'dykes' of differing magnetisation. The method assumes that every one of the 'dykes' extends to infinity in directions perpendicular to the profile, as well as vertically downwards. The upper termination of the 'dykes' is the basement surface. The depth to this surface is estimated by passing a short window along the magnetic profile, estimating a depth for each position of the window. The depth can be estimated from a value of the single autocorrelation at a single lag. In practice the first lag ( $n=1$ ) is used to estimate depth, while higher lags ( $n=2,3,4$ ) are used to check the validity of the depth estimate.

The Euler 3D deconvolution method (Reid *et al.* 1990, Geosoft 1994c) was used to estimate the depth to sources from both aeromagnetic and gravity sources. Euler's homogeneity equation relates the potential field (either magnetic or gravity) and its orthogonal components to the location of the source, given an assumed rate of change of the field with distance. This rate of change (degree of homogeneity) can be interpreted as a structural index (Thompson 1982) describing the form of the source structure as follows:

Table 3. Structural indices for Euler 3D deconvolution

Structural index	Structure (Magnetic field)	Structure (Gravity field)
0.0	contact	dyke/sill/step*
0.5	thick step*	ribbon
1.0	dyke/sill	pipe
2.0	pipe	sphere
3.0	sphere	-----

\* structures found to be most appropriate

The method has the advantages of being (1) applicable to anomalies caused by a wide variety of geological structures and (2) independent of remanent magnetisation and ambient field direction.

There are, however, a number of disadvantages surrounding the Euler 3D deconvolution method. Firstly, from a practical point of view, the computer implementations of the method generally produce many hundreds or even thousands of depth solutions for a single total field anomaly grid. This sounds like an advantage, however a substantial portion of the depth solutions may be unacceptable for a number of reasons. For example, depth solutions obtained for a total magnetic field grid using a structural index of 0 (contact) might be quite satisfactory for a number of magnetic anomalies, however it might be entirely inappropriate for other anomalies associated with, perhaps, more complicated structures such as dykes or sills (1.0). This presents the practical problem of sub-setting computer files containing large numbers of depth solutions and combining them together.

Perhaps more difficult than this, it is usual if there are many grid cells spanning a single potential field anomaly to obtain many depth solutions for a small geographic area. The question arises: which of the solutions to accept as the most representative of the depth to source structure? Smethurst (1994) developed a computer algorithm to sift through the depth estimates and accept only those which are confirmed by others in their immediate vicinity. Similar logic was used in the analysis of Euler depths for NAS-94. Depth estimates with high errors or far from the point in the grid from which they were derived were rejected immediately. The remaining depth estimates were reduced in density to 4 in a circular area with 2 km radius by rejecting data furthest from the median value (of those data within the circle). An iterative approach was used to avoid unfortunate side effects in regions with rapid lateral changes in source depth. The remaining data were then filtered so that no 2 data lie closer together than 700 m. The filtered data were then displayed on Maps 1,7 & 10 and Figs. 6, 13 & 16. The original spatial density of depth estimates was determined and displayed in working map form in order to 1) check the 'focusing' of depths (which has a bearing on the suitability of the structural index used), and 2) to provide an overview of the lineaments defined by Euler depths.

The 3D Euler deconvolution method was applied both to the aeromagnetic and gravity data-sets. The aeromagnetic grid based on 2 km spaced profiles were of sufficient quality to yield reliable depths of 2 or more kilometres. The gravity grid was interpolated from marine profiles and land stations with spacing between 1 and 10 km. The quality of the gravity depth estimates is therefore spatially variable, and attention to this was paid during the derivation of the combined magnetic/gravity basement depth model.

### 4.3 Forward modelling

We have carried out forward modelling of the gravity field along the profiles TB-38-87, PROFILE D and PROFILE E and the magnetic field along the eastern-most part of Profile NAS-410 (Figs. 17-20). When computing the response from the model we have used the IMP5 computer program of Torsvik (1992). The basic model in this program comprises 2½ dimensional bodies, i.e. bodies of polygonal cross-section of finite length in the strike direction. A gravimetric interpretation of profile TB-38-87 was reported earlier by Olesen et al. (1993).

Constraints offered by seismic information have been used. Our interpretations of PROFILE D and E are modifications of the seismic interpretations of Blystad et al. (in press). Seismic interpretations were digitised and depth-converted using the interval stacking velocities (Table 4). The depth-converted seismic horizons were imported directly into the IMP5 programme package. These two gravity profiles are extended to the mainland to help define the regional gravity field. The depth estimates obtained from the autocorrelation and Euler methods were also used to constrain the models.

*Table 4. Interval stacking velocities (\*1000 m/s) applied in depth conversion of seismic profiles.*

Profile	TB-38-87	PROFILE D	PROFILE E
Unit			
Sea water	1.48	1.48	1.48
Tertiary	2.3	2.0	1.9
Cretaceous	4.5	2.7	2.5
Jurassic	6.0	3.6	3.2
Triassic-Permian	6.0	4.5	4.5

#### 4.4 Geophysical interpretation map

A combined structural interpretation and depth to basement map was produced (Map 10 and Fig. 16). The interpretation of depth estimates from both gravity and aeromagnetic data was carried out by interpolation and contouring (Map 10, Fig. 16). In areas where aeromagnetic and gravity data sets yield different depths to basement the gravity interpretation is given the highest weight, especially in areas where we expect to find low-magnetic basement continuing from the on shore area. The quality of the gravity estimates varies according to the spacing of the local marine gravity profiles and this fact has to be taken into account in the contouring. Contouring was guided by the residual gravity map (Map 7, Fig. 13). High frequency anomalies interpreted to represent magnetic volcanics in the area to the west of the Nordland Ridge (Olesen & Smethurst 1994) are excluded from the basement model. Hand-drawn depth contours were digitised and then interpolated to a regular grid using the minimum curvature method with a tension factor of 0.2 (Map 10 and Fig. 16). Selected depth estimates from the gravity and aeromagnetic interpretation (section 4.2) are plotted on Map 10 in order to demonstrate the foundation in data for the interpretation.

The high-frequency anomalies were classified according to trend and possible cause (section 5.3). Regional fault zones and an area of high frequency, irregular anomalies possibly representing magnetic volcanics along the Bivrost (Lofoten) Lineament are marked.



## 5 INTERPRETATION AND DISCUSSION

### 5.1 General aeromagnetic and gravity features

The long wave-length component of the free air gravity field (Fig. 11) is interpreted in terms of a Moho topography (Figs. 18-20). There is a striking contrast between the interpreted Moho depths along the three profiles. Modelling of the northernmost and southernmost profiles, TB-38-87 (Fig. 18) and PROFILE E (Fig. 20), respectively, indicate a simple Moho surface with a thinning of the crust at the transition from the continent/platform area to the Vøring Basin. Conversely, modelling of PROFILE E, located between the two previous profiles, shows a shallower Moho (c. 18 km) below the Utgard High/Træna Sub-basin area, similar in form to the Moho below the Lofoten area (Mjelde et al. 1993, Olesen et al. 1993). This is consistent with interpretations of seismic data (Planke et al. 1991).

The magnetic anomaly pattern is interpreted to reflect three different types of magnetic sources; A) Magnetic basement in the Lofoten Horst, Nordland Ridge, southern central part of the Trøndelag Platform and mainland Norway, B) buried magnetic sedimentary rocks, sub-cropping sedimentary units and possible magnetic fault zones, C) Quaternary overburden of varying thickness and bathymetric features. Type A anomaly is described in section 5.2 and type B and C are described in section 5.3. The anomalies are identified and displayed on Maps. 7 & 10 and Figs. 13 & 16.

The aeromagnetic and gravity anomalies of the Lofoten-Vesterålen and the adjacent offshore area trend NE-SW and to a lesser extent NW-SE and ENE-WSW. The most prominent positive anomalies on Maps 7 & 8 (Figs. 13 & 14) correspond to the Røddøy, Grønøy and Sør Highs on the Nordland Ridge and the southernmost extensions of the Utrøst Ridge, Lofoten High, and Marmæle Spur. Negative anomalies represent the Træna Sub-basin and Vestfjorden Basin.

The well known Bivrost (Lofoten) Lineament and Ylvingen Fault Zone are located within the NAS-94 area. We were able to identify these features on our Maps 2 & 4 (Fig. 7 & 9). The Ylvingen Fault Zone can be traced across the continental shelf and onto land in the Ranafjord area (Maps 2 & 7 and Figs. 7 & 13) indicating that this Cretaceous structure follow an older NE-SW trending zone of weakness.

## 5.2 Depth to basement

The regional basement-related anomalies lie parallel to the Caledonian trend on land as well as to the principal direction of the offshore Mesozoic structures. The most prominent positive aeromagnetic and gravity anomalies on Maps 1 & 7 (Figs. 6 & 13) correspond to parts of the Nordland Ridge, the southernmost part of the Trøndelag Platform, the Lofoten High and the Sjøna tectonic window north of Ranafjorden. The two latter regional anomalies represent outcropping crystalline basement and are situated within the Transscandinavian Granite-Porphyry Belt (Gaal & Gorbatshev 1987) which continues below the Caledonian nappes all the way to southern Sweden (Henkel & Eriksson 1987). The high magnetite content of the Lofoten basement rocks is partly caused by mangeritic intrusives and partly by subsequent high grade metamorphism adjacent to the intrusives (Schlinger 1985, Olesen et al. 1991). Negative anomalies represent the central part of the Vestfjorden Basin to the north and the Helgeland Nappe Complex to the south of Ranafjorden. The latter continues from the mainland to the offshore area.

Some of the depth estimates along the Nordland Ridge are consistent with what is known from reflection seismics and exploration drilling, for instance on the Dønna Terrace and the northern part of the Nordland Ridge. Our depth estimates in these two areas vary between 4 and 7 km. The depth to magnetic basement on the central Nordland Ridge, however, exceeds the depth to crystalline basement obtained from exploration drilling. The 6609/7-1 well by Phillips Petroleum hit basement at a depth of 1.96 km while the depth-estimates from our study show that the magnetic basement is located at a depth of 7-9 km, indicating that the uppermost part of the basement is low-magnetic, as are some of the basement rocks on land, e.g. the Helgeland Nappe Complex (Table 1 & Mørk & Olesen 1995). The depth estimates of 7-9 km are similar to those calculated by (Åm 1970) from the old NGU data.

The depth to magnetic basement on both flanks of the Helgeland Basin lies between 8 and 10 km. The southern flank is a lineament representing the northward termination of a large magnetic body situated at a depth of 8-10 km in the Trøndelag Platform. This regional lineament coincides with the Vega High, indicating that this late Mesozoic structure is governed directly or indirectly by a more deeply seated structure. Deep seismic profiling during the Mobil Search Project indicated that this may indeed be the depth to the crystalline basement in this area. The thick sedimentary sequence most likely is a Devonian basin associated with the gravity collapse of the Caledonian Orogen. The above mentioned high amplitude (220 nT) regional anomaly (Map 1) is comparable in size and parallel to the Roan anomaly on the Fosen Peninsula 100 km to the south and could therefore have a similar cause. The magnetic rocks in Roan were formed during Caledonian high-grade metamorphism (Skilbrei et al. 1991) and were most likely uplifted during the Devonian orogenic collapse. We have applied measured magnetic properties (Skilbrei et al. 1991) of the basement rocks from the Roan area (susceptibility;  $20000 \times 10^{-6}$  SI, Q-value; 0.25) in the magnetic modelling of the Trøndelag Platform anomaly in Fig. 17.

Estimates of depths to basement from gravity data are often shallower than estimates from magnetic data in the same area (Map 10, Fig 20). Interpretation of depth to basement from gravity and aeromagnetic data reveals a depth of 6 - 8 km and 8 - 12 km, respectively, in the central part of the Helgeland Basin. This phenomenon may be due to either low-magnetic basement (equivalent of the Helgeland or Rødingsfjell Nappe Complexes on the mainland) or sediments of similar density as the underlying crystalline basement. The former seems to be the case on the Rødøy High along the Nordland Ridge where depths to magnetic basement exceed basement depths obtained from exploration drilling. In the forward modelling of gravity data along Profile D using constraints from reflection seismics and densities from Table 2, the basement of the Trøndelag Platform must be 2 km shallower than interpreted from the seismic profile (4.5 versus 6.5 km). The basement reflector is, however, not well defined in these profiles. The combined interpretation of the basement topography (Map 10 & Fig 16) reveal a central north-south trending ridge at a depth of approximately 5 km separating the Helgeland Basin into two 6-7 km deep sub-basins. A gravity anomaly caused by this ridge is visible on the free air and Bouguer gravity maps (Maps 5 - 8 & Figs. 11 - 14).

The combined interpretation of depths to basement from gravity and aeromagnetic depth estimates indicates a complex system of fault blocks along the Nordland Ridge. The depth to the basement is calculated to 9 - 12 km in of the Træna Sub-basin. Shallower magnetic sources at depths of 5 - 7 km in the southern part of the sub-basin may represent magnetic sills or volcanics. The southern part of the Vestfjorden Basin is an 7 - 8 km deep half graben defined by a boundary fault along the western margin as also shown by Brekke & Riis (1987). The northern part of the Vestfjorden Basin (to the north of the NAS-94 area), however, is a shallower (approximately 2 km deep) half graben with the boundary fault along the eastern margin of the basin (Olesen et al. 1993). A similar shift of polarity is also seen offshore Lofoten and Vesterålen where the faults shift from throwing down to the northwest to downthrow to the southeast, respectively.

### **5.3 High frequency aeromagnetic anomalies**

There are three distinct sets of high frequency anomalies caused by intra-sedimentary sources. The most pronounced set of these high frequency anomalies trends NNE-SSW (parallel to the coast) and coincides with sub-cropping Tertiary, Mesozoic and Late Palaeozoic sequences. The asymmetry of the anomalies – with a steep gradient and a negative anomaly to the east and a more gentle gradient to the west (Map 8 of Olesen & Smethurst 1994) shows that the sources of the anomalies dip gently towards the west, consistent with interpretations of seismic data (Rokoengen et al. 1988). The most distinct of the anomalies represents ‘unit X’ on the IKU bedrock geology map of the Mid Norwegian Shelf (Rokoengen et al. 1988). The ‘unit X’ sandstone was assigned a Miocene age by IKU while T.E. Eidvin (pers. comm. 1994) re-dated it to be of early Oligocene age. The older unit termed IX causes a weaker banded anomaly pattern which appears on our

maps (Maps 1, 2 & 10 and Figs. 6, 7 & 16). The susceptibility measurements on IKU's cores (Mørk & Olesen 1995) indicates that the positive coast-parallel anomalies are caused by 1) alternating beds of sandstone and claystone/siltstone/mudstone, 2) caliche and siderite-cemented sediments or 3) sediments containing iron-oxides (magnetite, ilmenite or haematite) or pyrrhotite. Negative anomalies are most likely caused by low-magnetic sandstones, gypsum or coal.

The second set of anomalies trends WSW-ENE (Map 1, 2 & 4) and coincides with the graben segments of the Ylvingen Fault Zone bounding the Vega High. Susceptibility measurements on cores from the IKU shallow drilling programme (Mørk & Olesen 1995) show that Lower Cretaceous claystones and siltstones have higher susceptibilities than Jurassic sandstones. A susceptibility contrast between the Cretaceous infill in the grabens along the Ylvingen Fault Zone and the juxtaposed Jurassic sandstones on both sides may explain the magnetic anomalies. A susceptibility contrast of  $200-300 \times 10^{-5}$  SI would produce the observed anomaly (Fig. 17) which means that the susceptibility of the Lower Cretaceous sediments within the grabens must be higher than the susceptibilities obtained from the IKU cores from the Nordland VI and VII areas ( $15-100 \times 10^{-5}$  SI; Mørk & Olesen 1995). There are two likely explanations of this lateral difference in susceptibility. 1) Increased content of siderite-cemented sediments or 2) Increased content of iron-oxides (magnetite, ilmenite or haematite) or pyrrhotite similar to the red-coloured sediments encountered in the IKU cores.

A splay of the Ylvingen Fault Zone seems to continue into Ranafjorden where Olesen et al. (1994) have reported evidence of recent faulting on land. There is also a striking coincidence between magnetic anomalies and other faults interpreted from seismic data on the Nordland Ridge and the Trøndelag Platform (superimposed on the aeromagnetic maps, e.g. Map 1, 2 & 4 and Figs. 6, 7 & 9).

The lowest amplitude anomalies (often less than 1 nT) trend WNW-ESE and occur on the Trøndelag Platform between the Træna Sub-basin in the west and the Nordland coast in the east. The only sedimentary unit on the shelf with such wide geographical distribution is the Quaternary overburden. These anomalies are best seen on the north-south horizontal magnetic gradient maps (Map 4, 14 & 15). Notice that on these maps the gradient on the southern flank of the WNW-ESE trending anomalies is *positive* and on the northern flank *negative*. Comparisons with the Quaternary deposits map of Rise et al. (1988) shows that, for example, the magnetic anomalies in blocks 6506/3, 6507/1 and 6507/2 coincide with thick sequences of overburden (Fig. 10). This increased thickness of the Quaternary overburden is also reflected in a more shallow bathymetry (Fig. 10). Some of the magnetic anomalies also coincide with other bathymetric features, such as in the Trændjupet area in the north (blocks 6611/4 and 6611/5). Our susceptibility measurements (Mørk & Olesen 1995) show that the overburden (especially glaciomarine clay) is frequently more magnetic than the underlying sediments. The magnetic carriers were identified as magnetite and/or haematite. Two higher amplitude anomalies with the same WNW-ESE trend in the Vestfjorden Basin south of the Lofoten Horst may, however, be caused by faults along the Bivrost (Lofoten)

Lineament. There are no indications of any coinciding bathymetric and Quaternary features in this area.

An area of irregular, high frequency anomalies occurs along the Bivrost Lineament (Map 9, Olesen & Smethurst 1994). The anomalies are interpreted to reflect Tertiary igneous intrusions and/or flows between the Bodø and Røst structural highs. A continuous belt of high frequency anomalies reflecting flow basalts and sills stretches from the western margin of the Bodø High northwards along the shelf edge to the west of the Utrøst Ridge and up to Andøya (Olesen et al. 1993). The area of irregular, high frequency anomalies along the Bivrost Lineament may represent a continuation of this belt. Shallower magnetic sources at depths of 5 - 7 km in the southern part of the Træna Sub-basin may represent magnetic sills or volcanics.

## **6 CONCLUSIONS**

1. The NAS-94 aeromagnetic survey is a state of the art data-set and has revealed several groups of high frequency anomalies not discernible in the old NGU data-sets. This is due to the use of more sensitive magnetometers, closer line spacing, more accurate navigation and improved processing and data presentation. The data have identified previously unknown geological structures and refined and extended the knowledge of known ones.
2. We have taken the interpretation of high sensitivity aeromagnetic data further by studying naturally occurring intra-formational anomalies and linking them as closely as possible with petrophysical measurements on actual sedimentary material of appropriate genera. We believe, then that we offer one of the first qualified accounts of intra-sedimentary anomalies.
3. When compared with petrophysical measurements on shallow cores from the IKU drilling programme, the anomaly pattern is interpreted to have three different types of magnetic sources; A) Quaternary overburden of varying thickness and bathymetric features, B) buried magnetic sedimentary rocks, sub-cropping sedimentary units and possible magnetic fault zones, C) magnetic basement in the Lofoten Horst, Nordland Ridge, southern part of the Trøndelag Platform and mainland Norway.
4. The sub-cropping wedge of Permian to Tertiary sediments along the inner Trøndelag Platform causes a distinct set of sub-parallel anomalies.
5. A correlation between anomalies caused by Early Cretaceous faulting on the Vega High and anomalies due to underlying basement topography indicates that the deep structural setting may have guided the location of the later faulting.

6. Estimates of depths to magnetic basement from gravity data are generally shallower than estimates from magnetic data in the same area.
7. The long wave-length component of the gravity field is interpreted in terms of Moho topography. The Moho is shallow (c. 18 km) below the Utgard High and Træna Sub-basin area, similar to the depths of the Moho below the Lofoten area.
8. Magnetic basement depths between 3 km and 13 km were obtained along the Nordland Ridge. There is, however, also evidence that a significant portion of the basement in this area is low-magnetic so that some depths to magnetic sources exceed basement depths obtained from exploration drilling. The combined interpretation of depths to basement from gravity and aeromagnetic data over the Nordland Ridge indicates a complex system of fault blocks.
9. Gravity and aeromagnetic methods yield depth estimates of 6 - 8 km and 8 - 12 km, respectively, for the central part of the Helgeland Basin. This discrepancy might also indicate either low-magnetic basement rocks under the basin (e.g. equivalent to the Helgeland or Rødingsfjell Nappe Complexes on the mainland) or sediments deep in the basin of similar density as the underlying crystalline basement. The former explanation is favoured.
10. A depth to the magnetic basement in the order of 10-11 km situated 40 km to the west of the outcropping crystalline basement on the Vikna Islands may be interpreted in terms of a deep sedimentary basin of Devonian age.
11. A splay of the Ylvingen fault on the Vega High seems to be continuous into the Ranafjorden area.
12. The depth to the basement is calculated to 9-12 km in the Træna Sub-basin and 7 - 8 km in the outer part of the Vestfjorden Basin.
13. Along the Bivrost (Lofoten) Lineament there is an area of irregular, high frequency anomalies interpreted as intra-sedimentary flow-basalts or sills.
14. The aeromagnetic data indicate that the Precambrian rocks in the Lofoten Horst are continuous below the Vestfjorden Basin as far as the Sjøna tectonic window to the north of Ranafjorden and constitute part of the Transscandinavian Granite-Porphyry Belt.
15. The modelling of intra-sedimentary magnetic anomalies is of prime importance and therefore is an issue which NGU will be concentrating on in future years and projects.

## 7 ACKNOWLEDGEMENTS

The NAS-94 project was financed by Mobil Exploration, Norsk Hydro, Statoil and the Geological Survey of Norway. Ola Kihle and Jomar Gellein produced the bathymetric/topographic map. Erik Henriksen and Tormod Henningsen (Statoil), Pål Haremo and Svein Viggo Johansen (Norsk Hydro) and Jon Roberts (Mobil Exploration) gave advice and consultation during the interpretation phase. Eirik Mauring critically read the report and made suggestions towards its improvement. We express our sincere thanks to all these persons.

## 8 REFERENCES

- Blystad, P., Færseth, R.B., Larsen, B.T., Skogseid, J. & Tørudbakken, B. in press: Structural elements of the Norwegian continental shelf, Part 2. The Norwegian Sea. *Nor. Petr. Dir. Bull.* 6.
- Brekke, H. & Riis, F. 1987: Tectonics and basin evolution of the Norwegian shelf between 62° and 72°N. *Nor. Geol. Tidsskr.* 67, 295-322.
- Bukovics, C. & Ziegler, P.A. 1985: Tectonic development of the Mid-Norway continental margin. *Marine and Petrol. Geology* 2, 2-22.
- Bøen, F., Eggen, S., and Vollset, J. 1984: Structures and basins of the margin from 62 to 69°N and their development. In A.M. Spencer et al. (eds.) Petroleum geology of the North European Margin, Norwegian Petroleum Society. *Graham and Trotman, London*, 253-270
- Cordell, L., Phillips, J.D. & Godson, R.H. 1992: U.S. Geological Survey potential-field geophysical software version 2.0. *USGS Open-file Report*.
- Gaal, G. & Gorbatshev, R. 1987: An outline of the Precambrian evolution of the Baltic Shield. *Precambrian Research* 35, 15-52.
- Gabrielsen, R.H., Færseth, R.B., Hamar, G. & Rønnevik, H. 1984: Nomenclature of the main structural features on the Norwegian continental shelf north of the 62nd parallel. In A.M. Spencer et al. (eds.) Petroleum geology of the North European Margin, Norwegian Petroleum Society. *Graham and Trotman, London*, 41-60.
- Geosoft 1994a: Geosoft mapping and processing system. Users manual. 391 pp.
- Geosoft 1994b: MAGMAP, 2-D frequency domain filtering. Users manual. 34 pp.
- Geosoft 1994c: GRIDEPTH, 3-D Euler deconvolution of potential field data. Users manual. 29 pp.
- Gustavson, M. 1981: Geologisk kart over Norge. Berggrunnskart MOSJØEN, M. 1:250 000. *Norges geologiske undersøkelse*.
- Gustavson, M. & Gjelle, S.T. 1991: Geologisk kart over Norge. Berggrunnskart MO I RANA, M. 1:250 000. *Norges geologiske undersøkelse*.
- Gustavson, M. & Blystad, P. in press: Geologisk kart over Norge. Berggrunnskart BODØ, M. 1:250 000. *Norges geologiske undersøkelse*.

- Gustavson, M. & Bugge, T. in press: Geologisk kart over Norge. Berggrunnskart VEGA, M. 1:250 000. *Norges geologiske undersøkelse*.
- Henkel, H. & Eriksson, L. 1987: Regional aeromagnetic and gravity studies in Scandinavia. *Precamb. Research* 35, 169-180.
- Kihle, O. 1992: THEMAMAP - et Uniras-basert produksjonssystem for fargerasterkart. *NGU Internal Report 92.068*. 172 pp.
- Mathisen, O. 1976: A method for Bouguer reduction with rapid calculation of terrain corrections. *Geographical Survey of Norway geodetic publications* 18, 40 pp.
- Mjelde, R., Sellevoll, M.A., Shimamura, H., Iwasaki, T. and Kanazawa, T. 1993: Crustal structure beneath Lofoten, N.Norway, from vertical incidence and wide-angle seismic data. *Geophys. Jour. Int.* 114, 116-126.
- Mørk, M.B. & Olesen, O. 1995: Magnetic susceptibility of sedimentary rocks from shallow cores off Mid Norway and crystalline rocks from the adjacent onland areas. NAS-94 Interpretation Report, Part II: Petrophysical data. *NGU Report 95.039*, 68pp
- Olesen, O., Henkel, H., Kaada, K. & Tveten, E. 1991: Petrophysical properties of a prograde amphibolite - granulite facies transition zone at Sigerfjord, Vesterålen, Northern Norway. In: P. Wasilewski & P. Hood (Eds.). Magnetic anomalies – land and sea. *Tectonophysics* 192, 33-39.
- Olesen, O., Torsvik, T.H., Tveten, E. & Zwaan, K.B. 1993: The Lofoten-Lopphavet Project - an integrated approach to the study of a passive continental margin, Summary report. *NGU Report 93.129*, 54 pp.
- Olesen, O., Gjelle, S., Henkel, H., Karlsen, T.A., Olsen, L. & Skogseth, T. 1994: Neotectonic studies in Ranafjorden area, northern Norway. *NGU Report 94.073*, 43 pp.
- Olesen, O. & Smethurst, M. 1994: NAS-94 Interpretation Report, Part I: Aeromagnetic data. *NGU Report 94.074*, 44 pp.
- Phillips, J.D. 1975: Statistical analysis of magnetic profiles and geomagnetic reversal sequence *Ph.D. thesis. Stanford University*, 134 pp.
- Phillips, J.D. 1979: ADEPT: A program to estimate depth to magnetic basement from sample magnetic profiles. *U.S. geol. Surv. open-file report 79-367*, 35 pp
- Planke, S., Skogseid, J. & Eldholm, O. 1991: Crustal structure off Norway, 62° to 70° north. *Tectonophysics* 189, 91-107.
- Reid, A.B., Allsop, J.M., Granser, H., Millett, A.J. & Sommerton, I.W. 1990: Magnetic interpretation in three dimensions using Euler deconvolution, *Geophysics* 55, 80-91.
- Rise, L., Rokoengen, K., Sættem, J. & Bugge, T. 1988: Thickness of Quaternary deposits on the Mid Norwegian Continental Shelf. Scale 1:1000 000. *IKU publ. 119. Continental Shelf and Petroleum Technology Research Institute A/S*.
- Rokoengen, K., Rise, L., Bugge, T. & Sættem, J. 1988: Bedrock geology of the Mid Norwegian Continental Shelf. Scale 1:1000 000. *IKU publ. 118. Continental Shelf and Petroleum Technology Research Institute A/S*.



- Schlinger, C. M. 1985: Magnetization of lower crust and interpretation of regional magnetic anomalies: Example from Lofoten and Vesterålen, Norway. *J. Geophys. Res.* 90, 11484-11504.
- Skilbrei, J.R., Skyseth, T. & Olesen, O. 1991: Petrophysical data and opaque mineralogy of high-grade and retrogressed lithologies: implications for the interpretation of aeromagnetic anomalies in Northern Vestranden, Central Norway. In: P. Wasilewski & P. Hood (Eds.). *Magnetic anomalies – land and sea. Tectonophysics* 192, 21-31.
- Smethurst, M. 1994: Viking-93 aeromagnetic survey: Interpretation report. *NGU Report 94.011*, 63 pp.
- Solli, A., Bugge, T. & Thorsnes, T. in press: Geologisk kart over Norge. Berggrunnskart NAMSOS, M. 1:250 000. *Norges geologiske undersøkelse*.
- Swain, C.J. 1976: A Fortran IV program for interpolating irregularly spaced data using the difference equations for minimum curvature. *Computers & Geosciences* 1, 231-240.
- Telford, W.M., Geldart, L.P., Sheriff, R.E. & Keys, D.A. 1976: Applied Geophysics. *Cambridge University Press, Cambridge. Cambridge*. 860 pp.
- Thompson, D.T. 1982: EULDPH: A new technique for making computer-assisted depth estimates from magnetic data. *Geophysics* 47, 31-37.
- Torsvik, T.H. 1992: IMP5 - Interactive modelling of potential field data (Release 5). *NGU Report 92.305*. 75 pp.
- Torsvik, T.H. & Olesen, O. 1992: PDEPTH - calculation of depth to magnetic basement from profile data. *NGU Report 92.212*, 26 pp.
- Åm, K. 1970: Aeromagnetic investigations on the continental shelf of Norway, Stad-Lofoten 62-69°N, *Nor. geol. unders.* 266, 49-61.

## List of figures and maps

- Fig. 1. Map of structural elements within the survey area (Blystad et al. in press).
- Fig. 2. Flight pattern diagram and map sheet layout (1:500.000 scale maps, Olesen & Smethurst 1994) of the aeromagnetic measurements.
- Fig. 3. Profile pattern diagram of marine gravity profiles and gravity stations on land. The Bouguer gravity field is displayed in colour (red - high, blue - low).
- Fig. 4. Regional field generated using a 100 km Gaussian low-pass filter (red - high, blue - low).
- Fig. 5. Sample locations, 4100 rock samples measured with respect to density, susceptibility and remanence and 1659 susceptibility measurements on cores from the IKU shallow drilling programme (14 offshore wells). The figure is a reduced version of the 1:1 mill. map of Mørk & Olesen (1995).
- Fig. 6. Total magnetic field anomaly map. A shaded relief effect emphasises shorter wavelength features. (Map 1 at a reduced scale.)
- Fig. 7. Magnetic gradient amplitude map (Analytical signal) black/white. (Map 2 at a reduced scale.)
- Fig. 8. North-south horizontal gradient map. (Map 3 at a reduced scale.)
- Fig. 9. Residual magnetic anomaly map produced by a 15 km Gaussian high-pass filter. (Map 4 at a reduced scale.)
- Fig. 10. A) A section of the N-S horizontal magnetic gradient map, covering blocks 6506/3, 6507/1 and 6507/2 (Map 3 and Fig. 8). B) Thickness of Quaternary deposits (Rise et al. 1988) for the area denoted in (A). There is a striking coincidence between the aeromagnetic anomalies and the Quaternary and bathymetric features. Susceptibility measurements on cores from the Quaternary overburden show that the glaciomarine clay is often magnetic.
- Fig. 11. Gravity anomaly map: free air at sea and Bouguer on land. (Map 5 at a reduced scale.)
- Fig. 12. Bouguer gravity anomaly map. (Map 6 at a reduced scale.)
- Fig. 13. Residual gravity field from a 100 km Gaussian filter and depth estimates to anomaly sources, based on both gravity and magnetic data. (Map 7 at a reduced scale.)
- Fig. 14. Residual gravity field from a 50 km Gaussian filter. (Map 8 at a reduced scale.)
- Fig. 15. Flight lines, bathymetry and topography. (Map 9 at a reduced scale.)
- Fig. 16. Geophysical interpretation map. (Map 10 at a reduced scale.)
- Fig. 17. A) Magnetic modelling of the eastern part of Profile NAS-410 traversing the Vega High. The magnetic anomalies coincide with the graben segments within the Ylvingen Fault Zone. B) is an enlargement of part of (A) shown by the dashed lines. The shape of the early Cretaceous graben infill is taken from seismic profile MN88-407. A susceptibility contrast of  $200 \times 10^{-5}$  SI (and a Q-value of 0.5) must be used to produce the observed anomaly. This is, however, higher than the measured susceptibility contrast between Jurassic sandstones and Lower Cretaceous silt- and clay-stones from the cores at IKU (maximum  $100 \times 10^{-5}$  SI). Lateral variations in susceptibility within the various units may explain the discrepancy.

Fig. 18a. Gravity interpretation along seismic profile TB-38-87 (Olesen et al. 1993) to a depth of 35 km. The densities used are shown in Table 2. The location of the profile is indicated on Maps 5-8 & 10 and Figs. 11-14 & 16.

Fig. 18b As Fig. 18a but to a depth of 10 km.

Fig. 19a. Gravity interpretation along seismic profile D (Blystad et al. in press.) to a depth of 35 km. The seismic interpretation from Blystad et al. (in press.) was digitised and depth-converted using the seismic velocities in Table 3. The applied densities are shown in Table 2. The location of the profile is shown on Maps 7 & 10. and Figs. 11-14 & 16. The most detailed interpretation is carried within the NAS-94 area (the Nordland Ridge and the Trøndelag Platform) while the interpretation in the Vøring Basin is more general.

Fig. 19b. An enlargement of part of Fig. 19a shown by the dashed lines, interpreted to a depth of 13 km.

Fig. 20a. Gravity interpretation along seismic profile E (Blystad et al. in press.) to a depth of 35 km. The seismic interpretation from Blystad et al. (in press.) was digitised and depth-converted using the seismic velocities in Table 3. The applied densities are shown in Table 2. The location of the profile is shown on Maps 5-8 & 10. and Figs. 11-14 & 16. The most detailed interpretation is carried within the NAS-94 area (the Nordland Ridge and the Trøndelag Platform) while the interpretation in the Vøring Basin is more general.

Fig. 20b. An enlargement of part of Fig. 20a shown by the dashed lines, interpreted to a depth of 13 km.

Map 1. Total magnetic field anomaly map in colour and high frequency (15 km Gaussian filtered) shaded relief map in black/white, Scale 1:500.000

Map 2. Magnetic gradient amplitude map (Analytical signal) black/white, Scale 1:500.000

Map 3. North-south horizontal gradient map, Scale 1:500.000

Map 4. Residual magnetic anomaly map (15 km Gaussian high-pass filtered), Scale 1:500.000

Map 5. Gravity anomaly map, free air at sea and Bouguer on land, Scale 1:500.000

Map 6. Bouguer gravity anomaly map, Scale 1:500.000

Map 7. Residual gravity field (100 km Gaussian filtered) and depth estimates to anomaly sources, Scale 1:500.000

Map 8. Residual gravity field (50 km Gaussian filtered) and depth estimates to anomaly sources, Scale 1:500.000

Map 9. Flight lines, bathymetry and topography, Scale 1:500.000.

Map 10. Geophysical interpretation map, Scale 1:500.000.

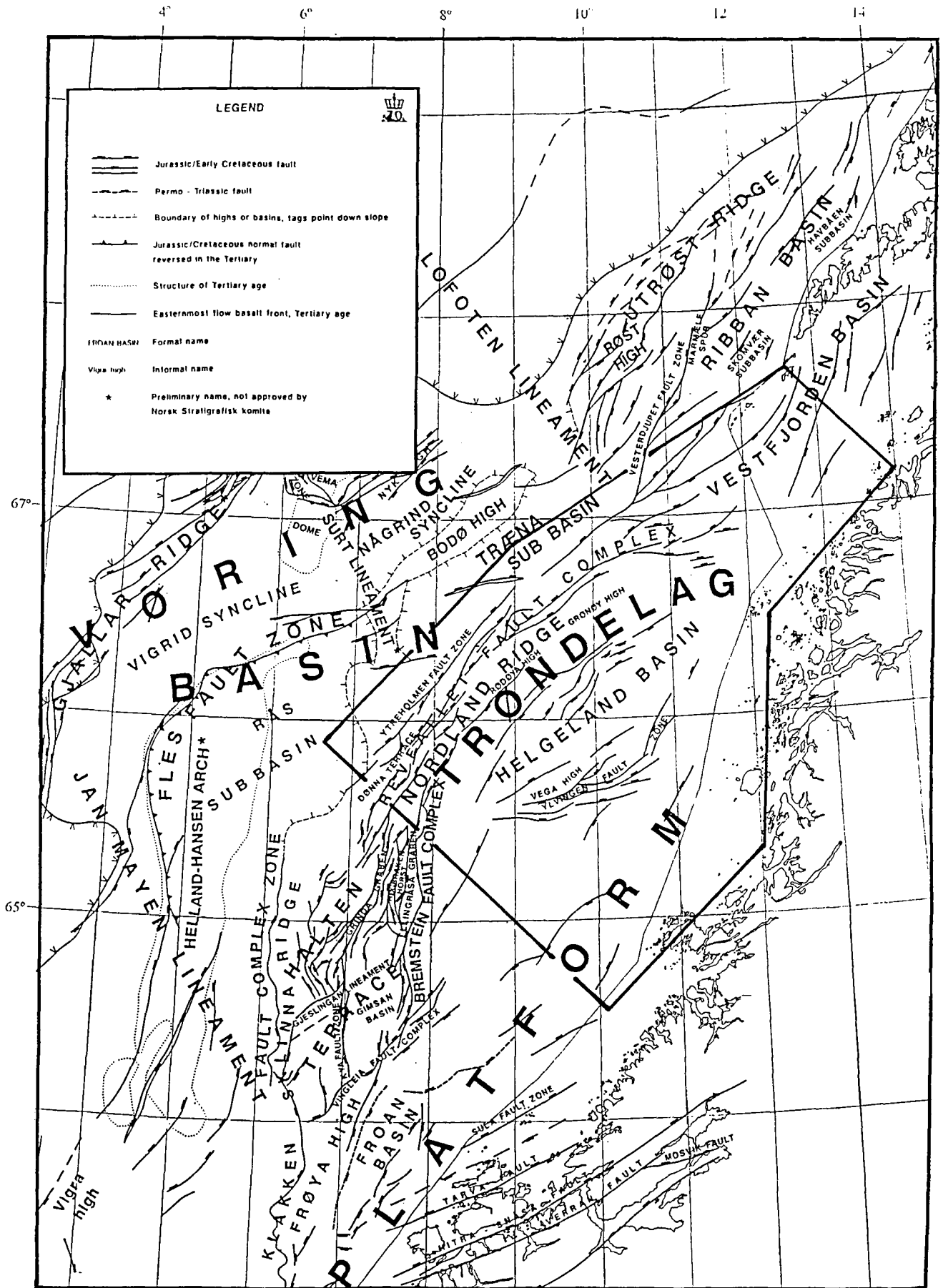


Fig. 1. Map of structural elements within the survey area (Blystad et al. in press).

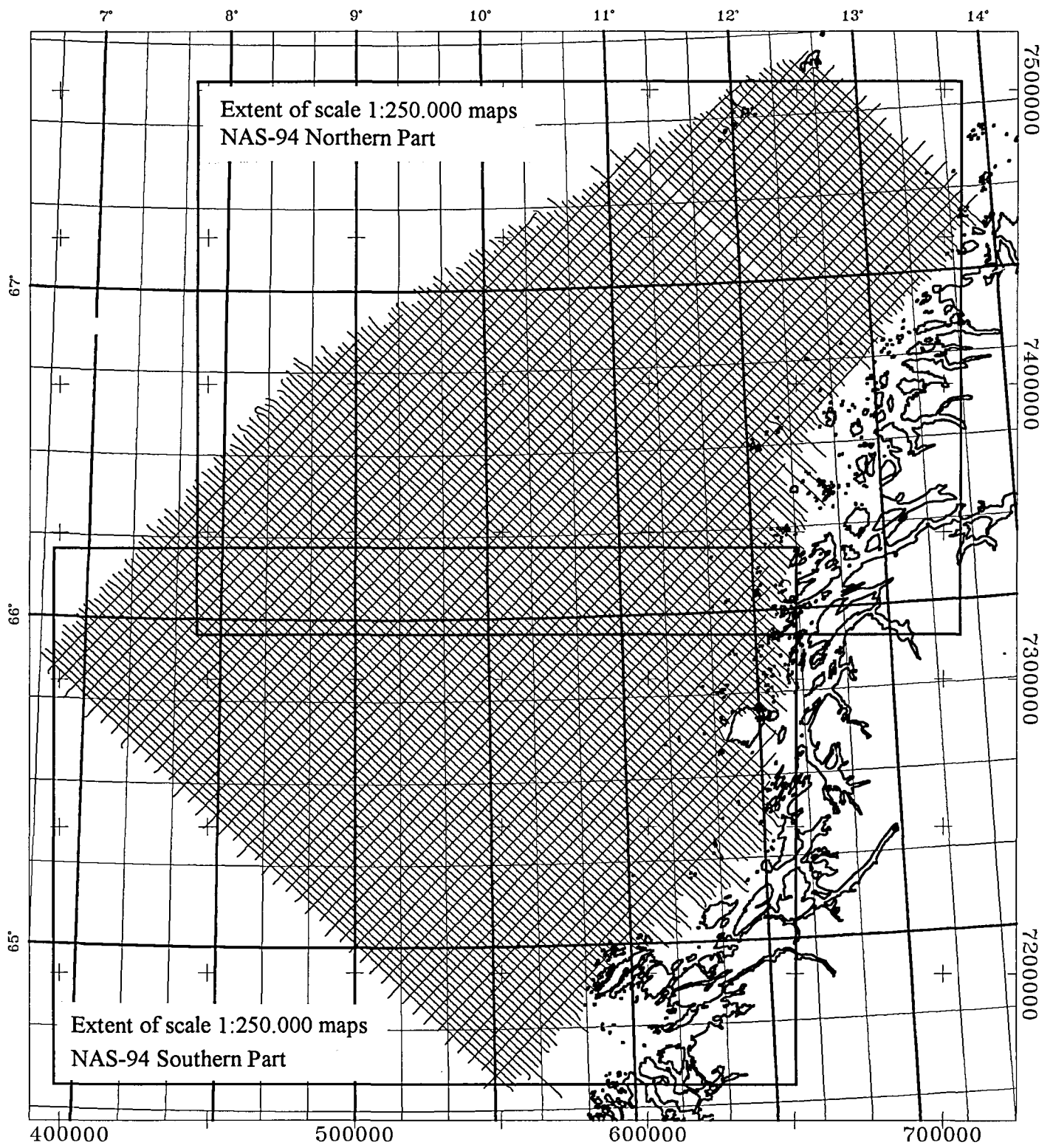
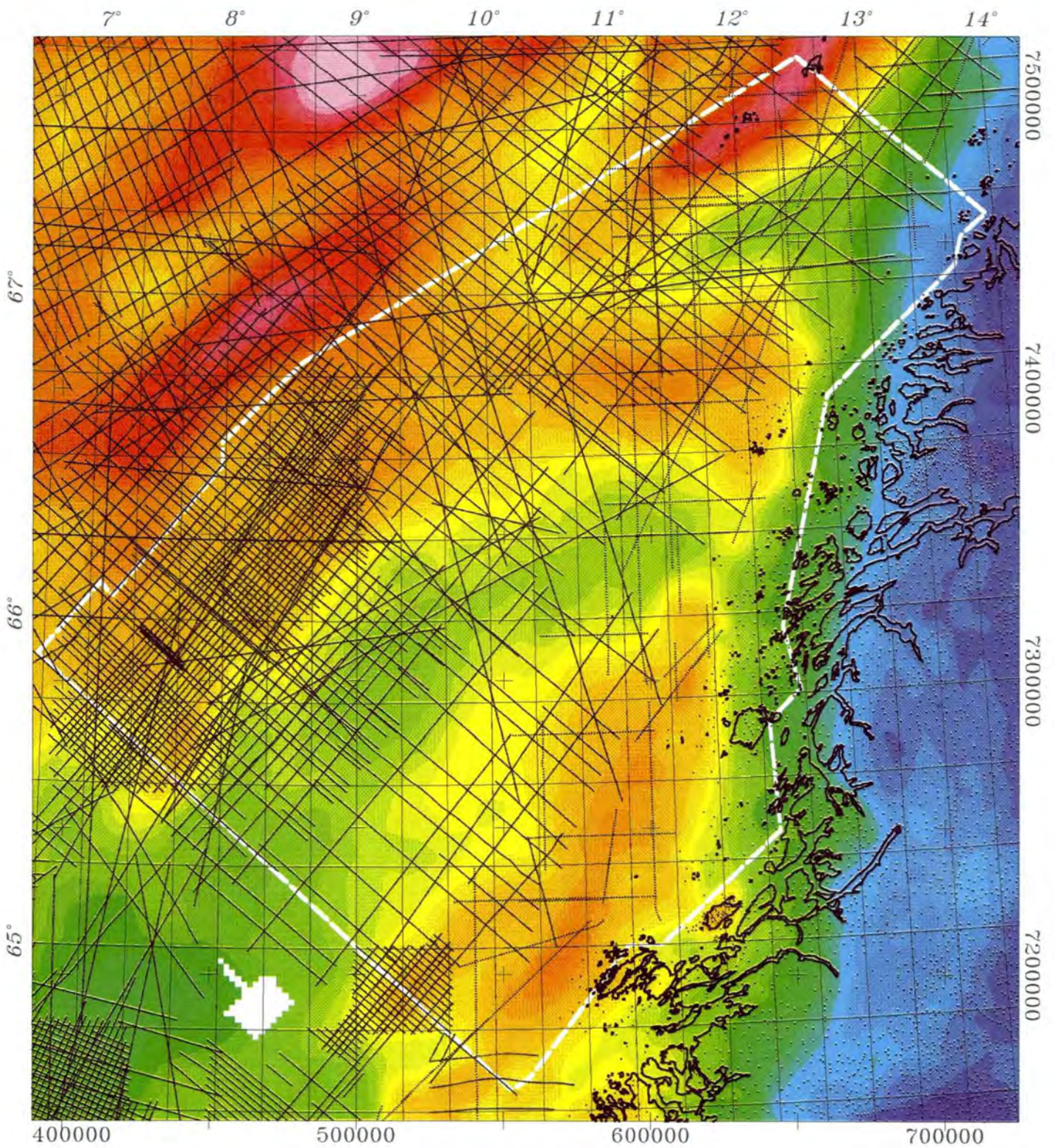


Fig. 2. Flight pattern diagram and map sheet layout of the aeromagnetic measurements.



*Fig. 3. Profile pattern diagram of marine gravity measurements and gravity stations on land. The Bouguer gravity field is displayed in colour (red - high, blue - low).*

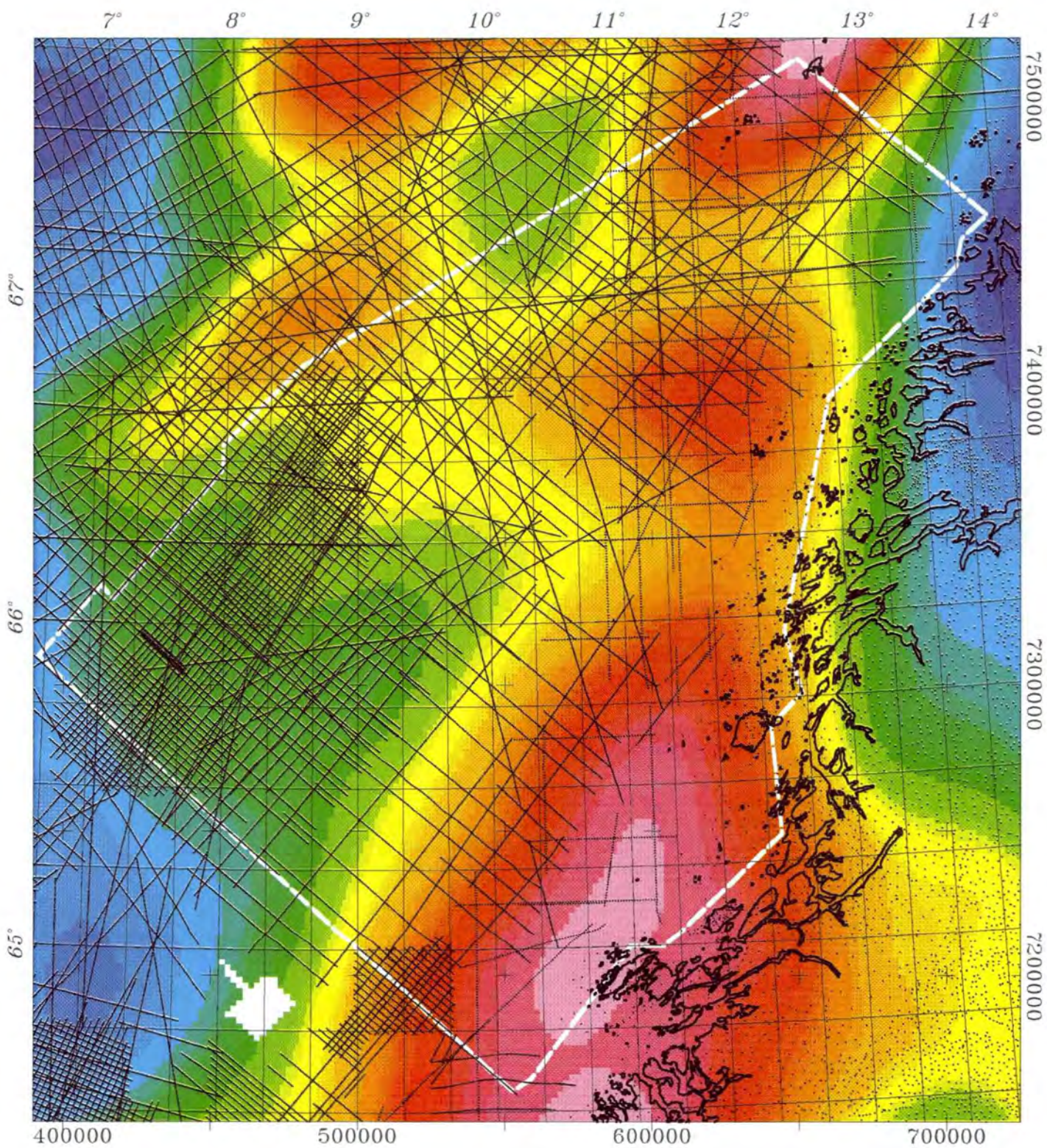


Fig. 4. Regional Bouguer gravity field generated using a 100 km Gaussian low-pass filter (red - high, blue - low).

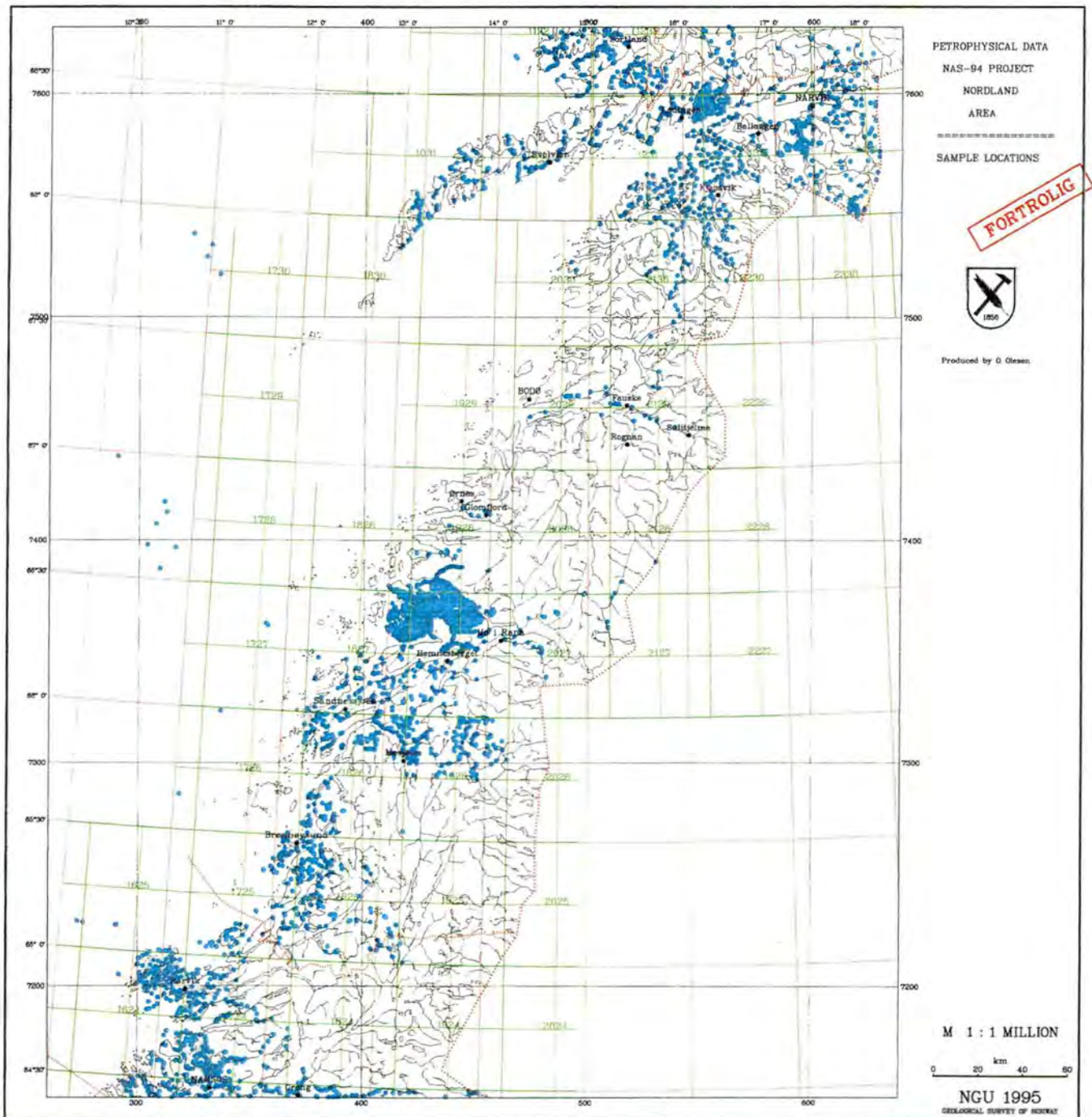
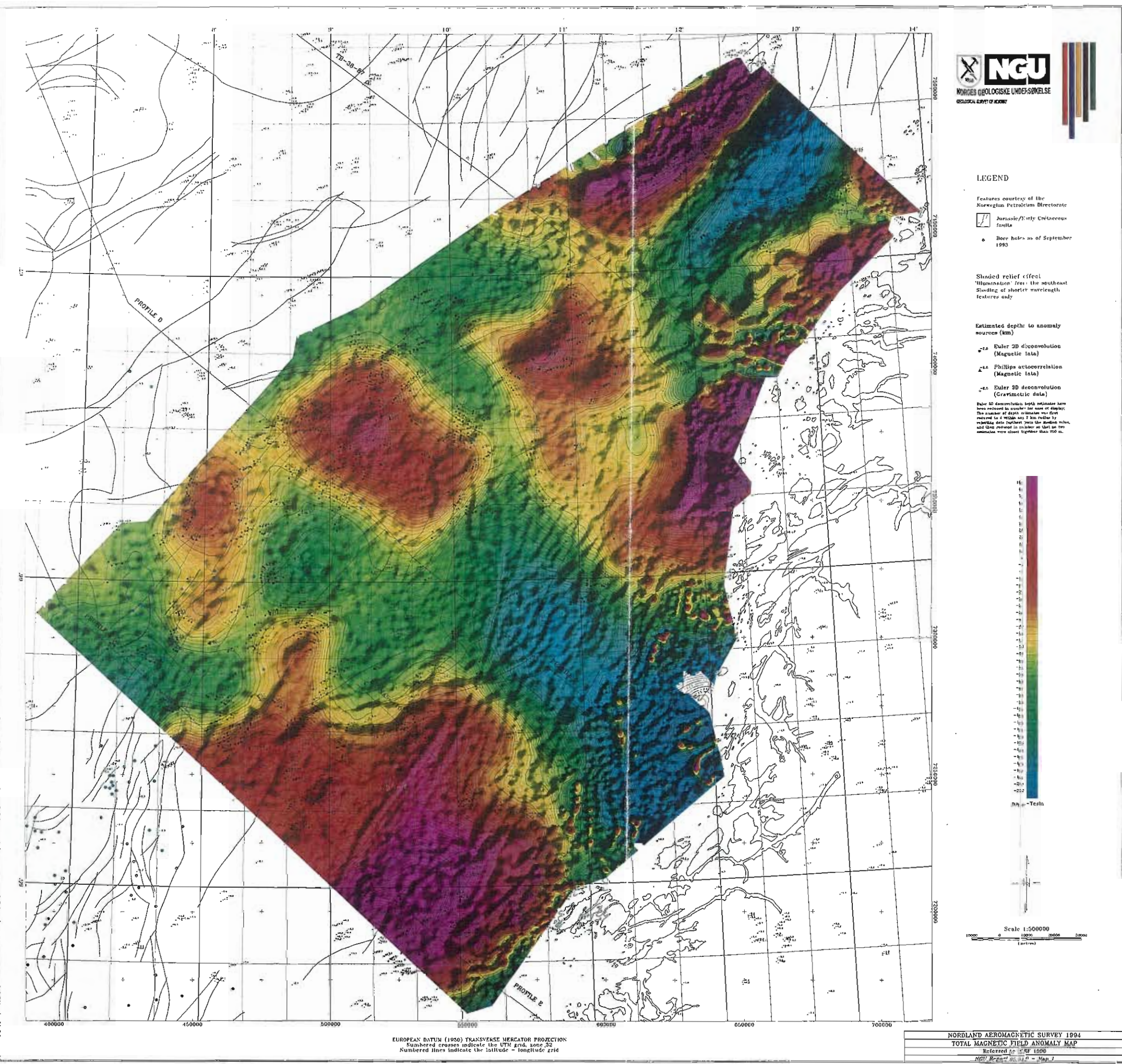


Fig. 5. Sample locations, 4100 rock samples measured with respect to density, susceptibility and remanence and 1659 susceptibility measurements on cores from the IKU shallow drilling programme (14 offshore wells). The figure is a reduced version of the 1:1 mill. map of Mørk & Olesen (1995).





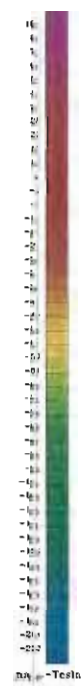
**LEGEND**

- Features courtesy of the Norwegian Petroleum Directorate
- Jurassic/Early Cretaceous faults
- Bore holes as of September 1993

Shaded relief effect  
 "Illumination" from the southeast  
 Shading of shorter wavelength features only

- Estimated depth to anomaly sources (km)
- Euler 3D deconvolution (Magnetic data)
  - Phillips autocorrelation (Magnetic data)
  - Euler 3D deconvolution (Cratonic data)

Euler 3D deconvolution depth estimates have been reduced to 50% of the true depth. The number of depth estimates was first reduced to a 100m x 100m grid by rejecting data further from the median value, and then reduced to 50% of that so the anomalies were closest together than 100 m.



EUROPEAN DATUM (1956) TRANSVERSE MERCATOR PROJECTION  
 Numbered crosses indicate the UTM grid, zone 32  
 Numbered lines indicate the latitude - longitude grid

NORLAND AEROMAGNETIC SURVEY 1994  
 TOTAL MAGNETIC FIELD ANOMALY MAP  
 Referred to as REF 1090  
 NGU Report 1000 - Map 1

Fig. 6. Total magnetic field anomaly map. A shaded relief effect emphasises shorter wavelength features. (Map 1 at a reduced scale.)

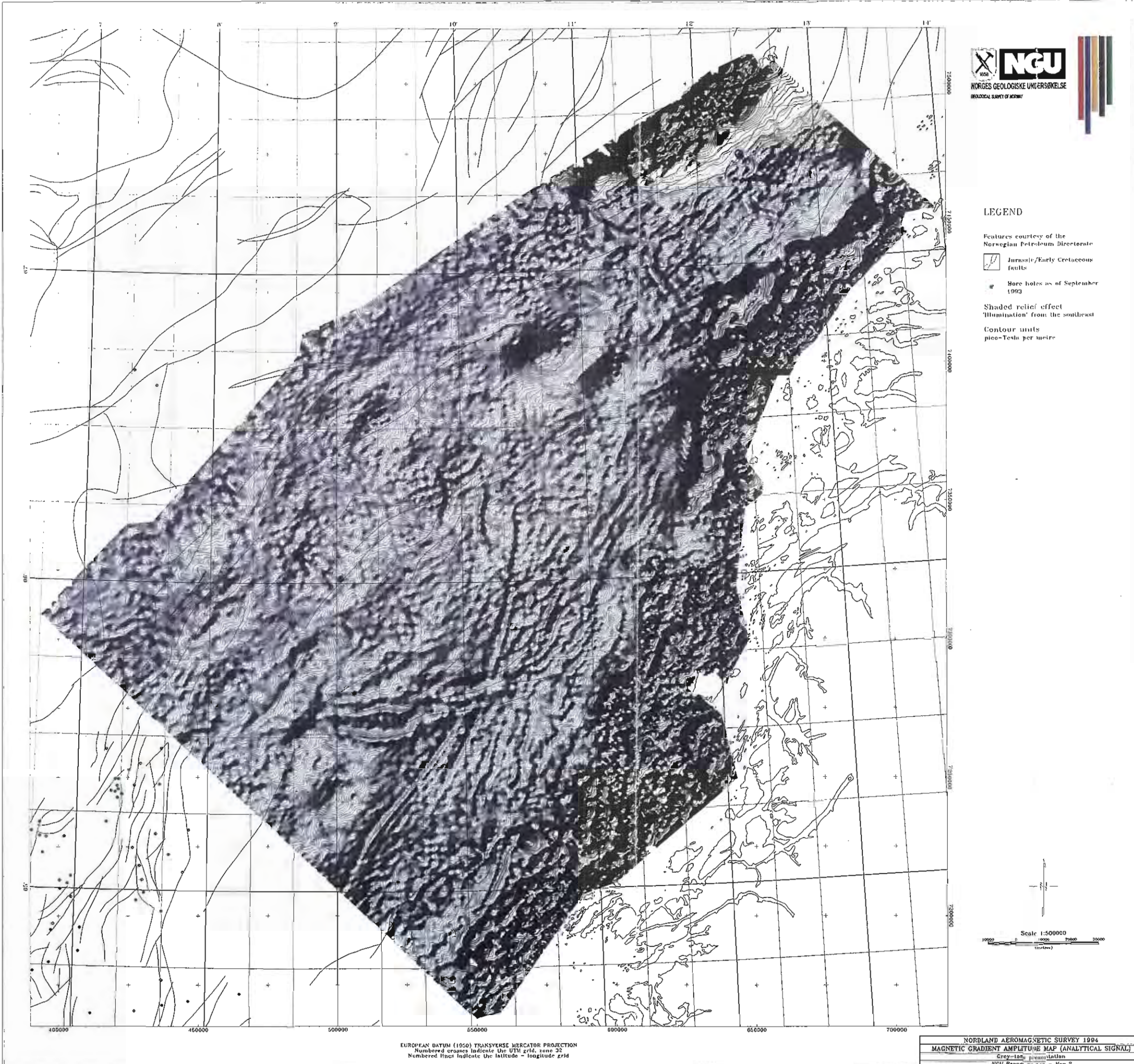


Fig. 7. Magnetic gradient amplitude map (Analytical signal) black/white. (Map 2 at a reduced scale.)

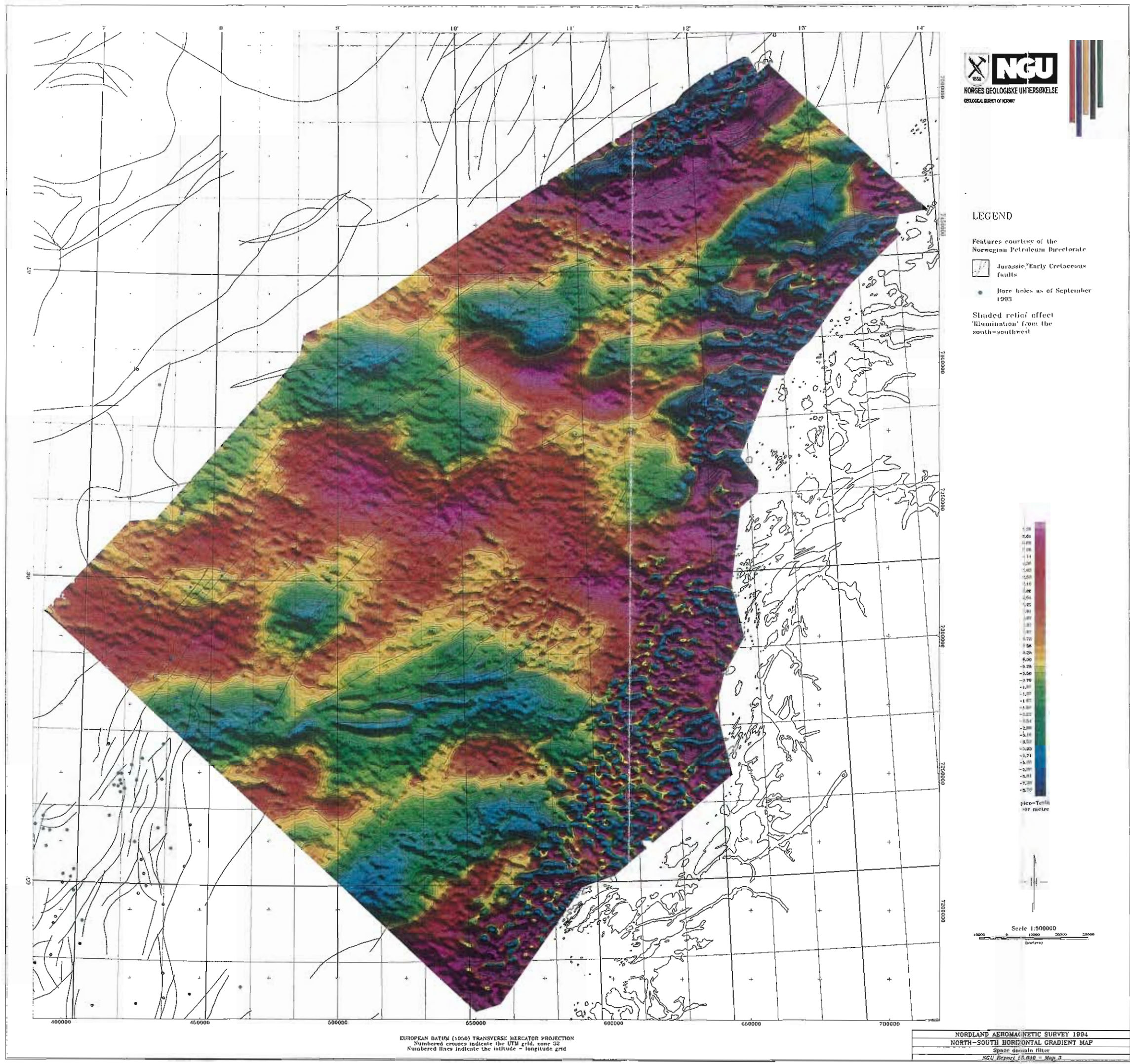


Fig. 8. North-south horizontal gradient map. (Map 3 at a reduced scale.)

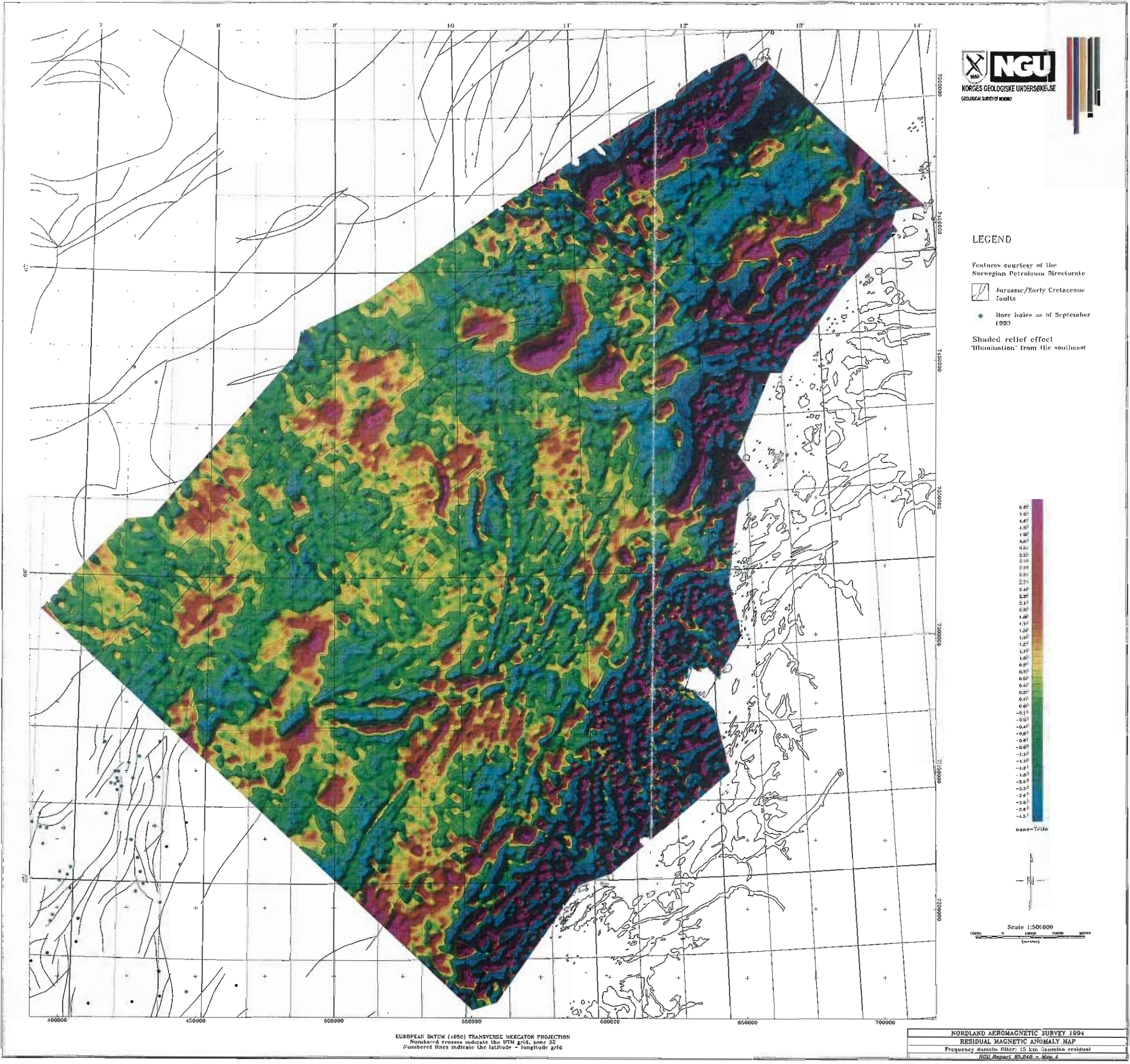
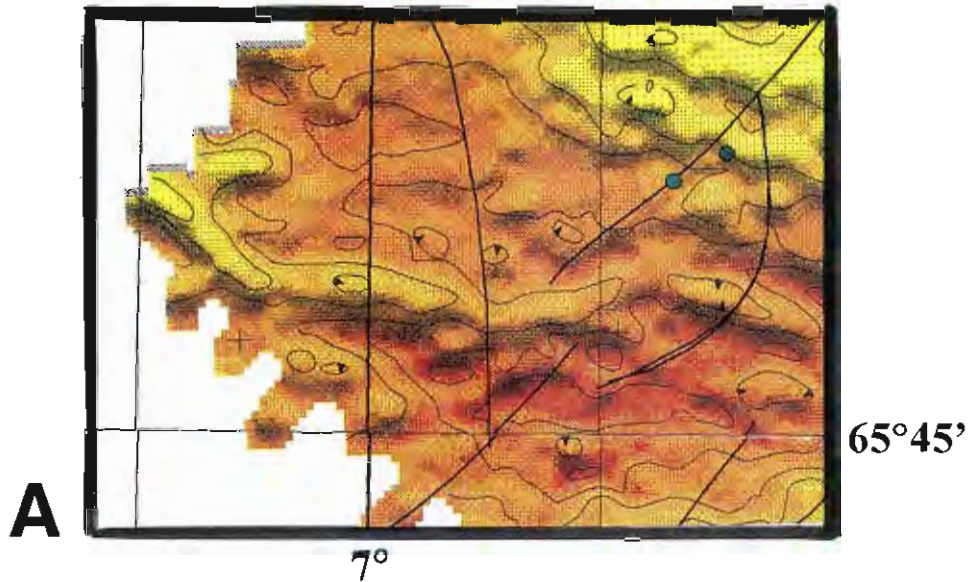


Fig. 9. Residual magnetic anomaly map produced by a 15 km Gaussian high-pass filter. (Map 4 at a reduced scale.)

**Horizontal magnetic gradient, N-S direction**



**Thickness of Quaternary deposits (ms)**

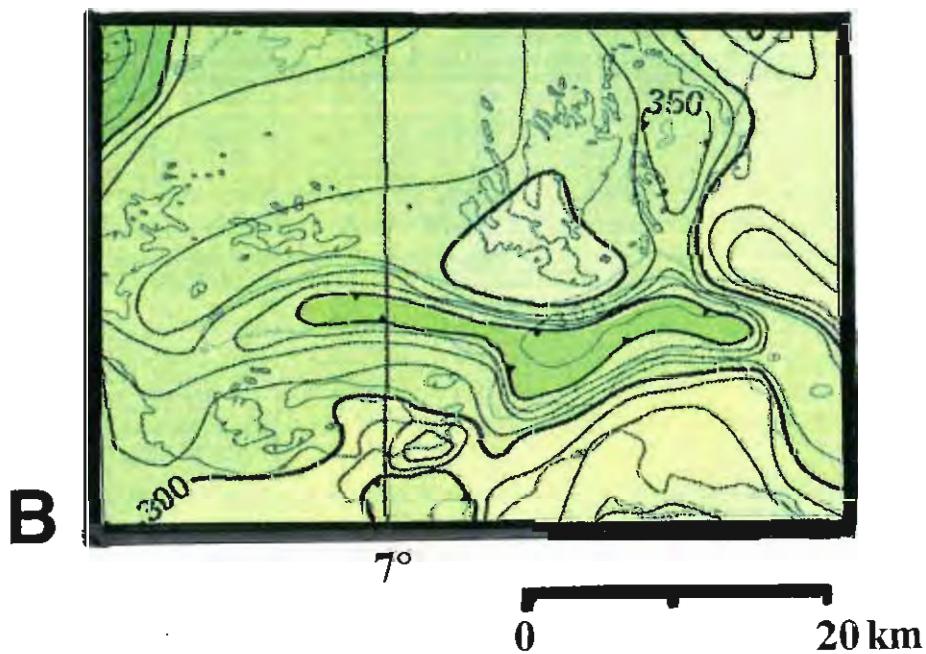


Fig. 10. A) A section of the N-S horizontal magnetic gradient map, covering blocks 6506/3, 6507/1 and 6507/2 (Map 3 and Fig. 8). B) Thickness of Quaternary deposits (Rise et al. 1988) for the area denoted in (A). There is a striking coincidence between the aeromagnetic anomalies and the Quaternary and bathymetric features. Susceptibility measurements on cores from the Quaternary overburden show that the glaciomarine clay is often magnetic.

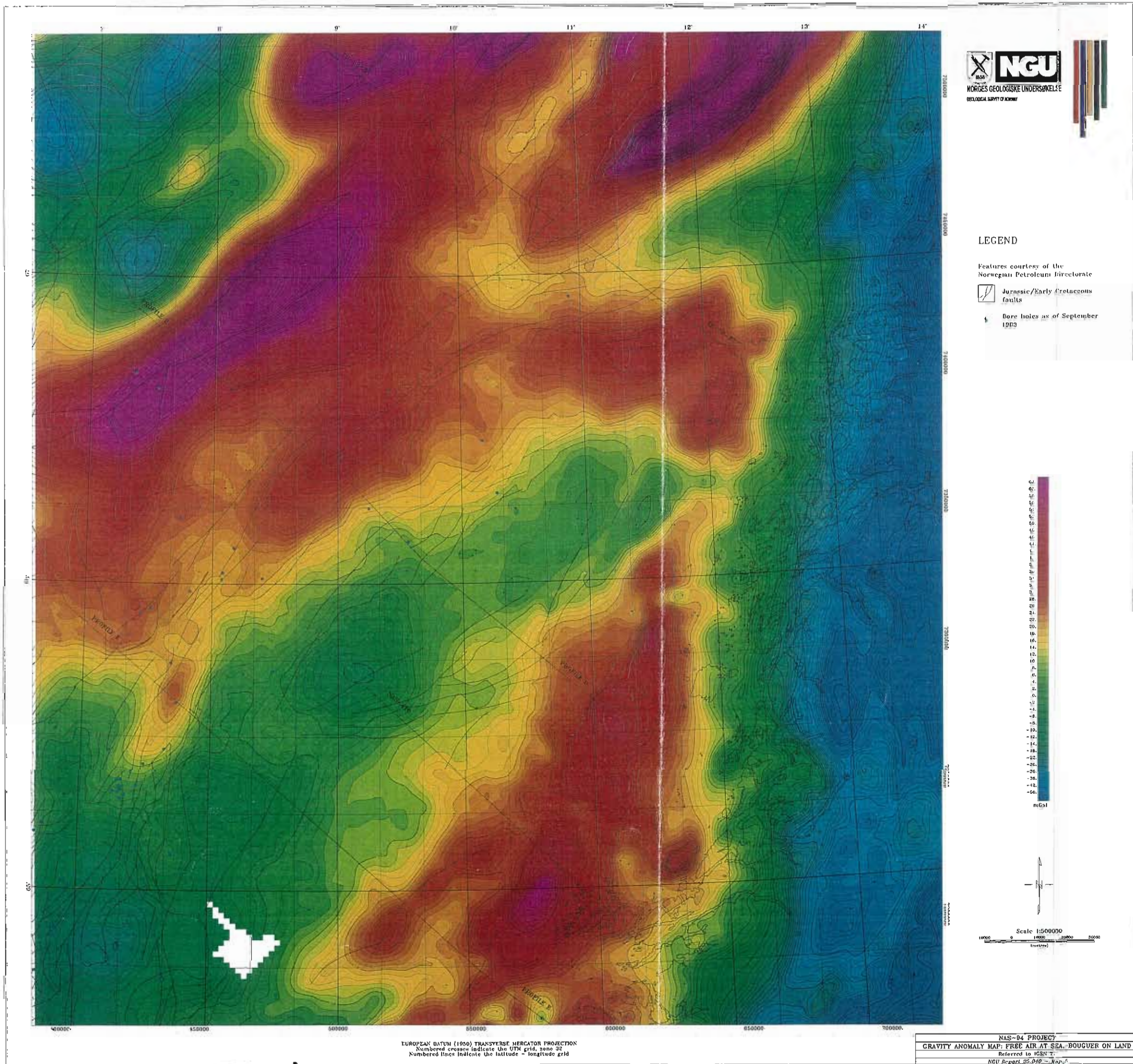


Fig. 11. Gravity anomaly map: free air at sea and Bouguer on land. (Map 5 at a reduced scale.)

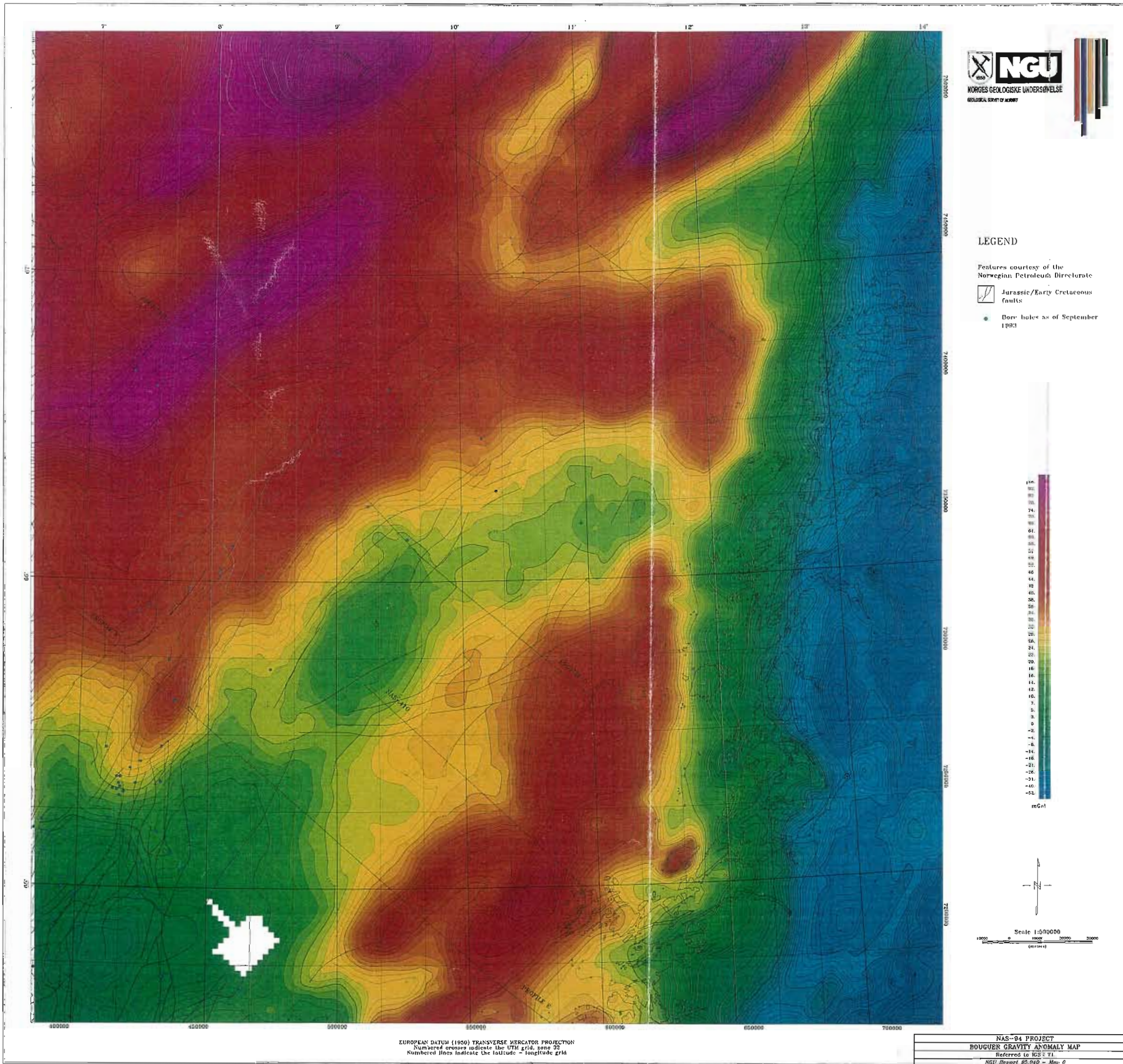


Fig. 12. Bouguer gravity anomaly map. (Map 6 at a reduced scale.)

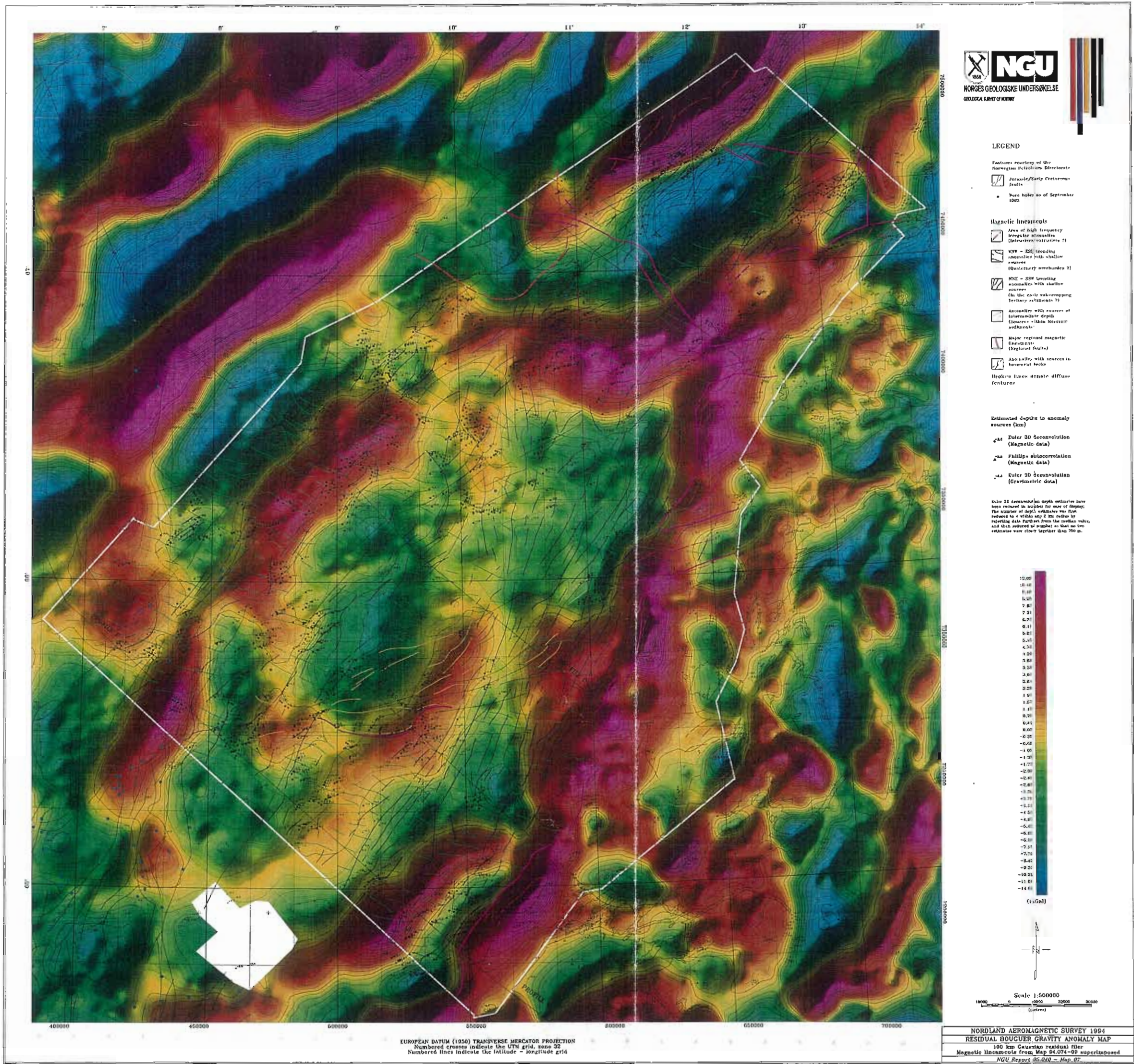
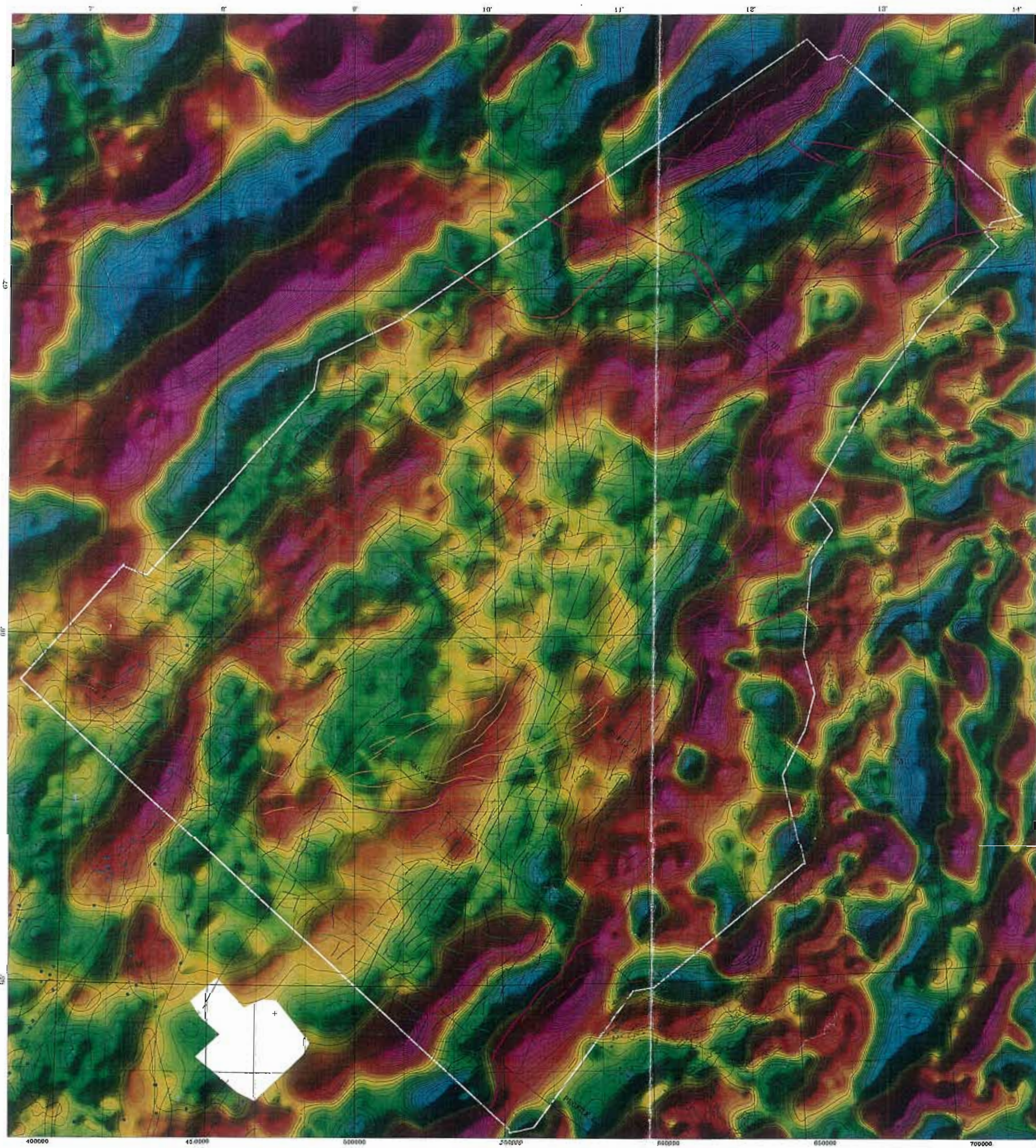
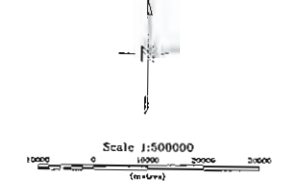
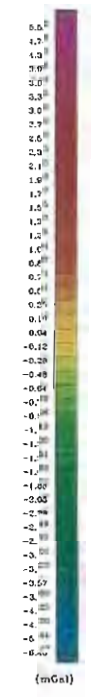


Fig. 13. Residual gravity field from a 100 km Gaussian filter and depth estimates to anomaly sources, based on both gravity and magnetic data. (Map 7 at a reduced scale.)





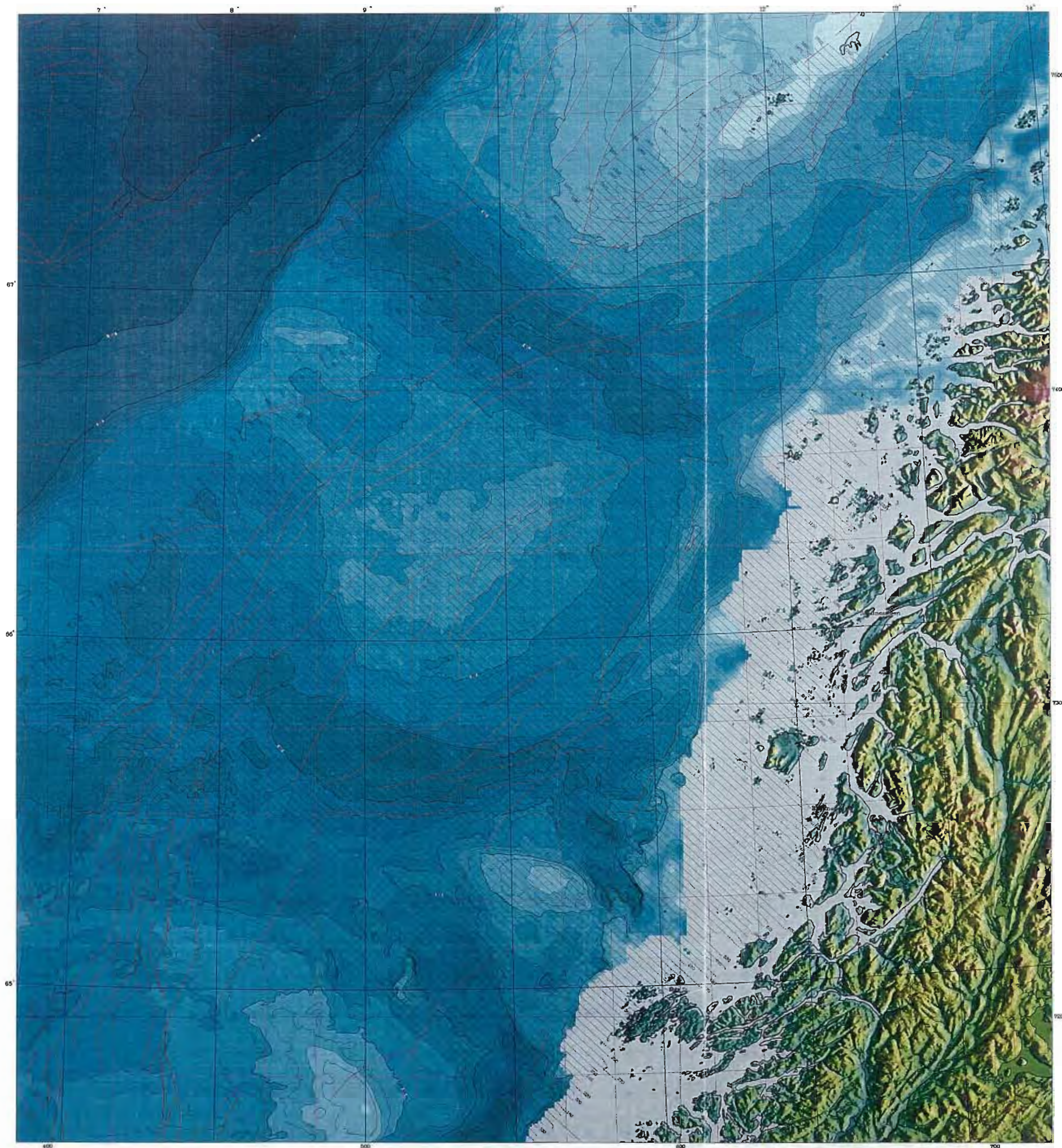
- LEGEND**
- Features courtesy of the Norwegian Petroleum Directorate
- Jurassic/Early Cretaceous faults
  - Bore holes as of September 1993
- Magnetic horizons**
- Area of high frequency irregular anomalies (Intra- or inter-tect. ?)
  - ENE - ESE trending anomalies with shallow sources (Quaternary overburden ?)
  - NSW trending anomalies with shallow sources (In the east sub-rapping Tertiary sediments ?)
  - Anomalies with sources at intermediate depth (Sources within Mesozoic sedimentary)
  - Major regional magnetic horizons (Regional faults)
  - Anomalies with sources in basement rocks
- Broken lines denote diffuse features



EUROPEAN DATUM (1950) TRANSVERSE MERCATOR PROJECTION  
 Numbers of crosses indicate the UTM grid zone 32  
 Numbered lines indicate the latitude - longitude grid

NORDLAND AEROMAGNETIC SURVEY 1994  
 RESIDUAL BOUGUER GRAVITY ANOMALY MAP  
 50 km Gaussian residual filter  
 Magnetic isograds from Map 84.074-09 superimposed  
 NGU Report 85.040 - Map 8

Fig. 14. Residual gravity field from a 50 km Gaussian filter. (Map 8 at a reduced scale.)



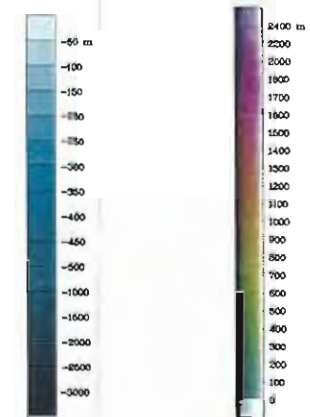
**Map description**

The bathymetry is plotted as an ordinary contour map in shades of blue with contour lines every 25 m down to 500 m and every 100 m for greater depths. Thicker lines are used for every 100 m down to 500 m and for every 500 m for greater depths.

A pseudocolor topographic with 'illumination' from the east is used for the topography.

Data were provided by the Norwegian Mapping Authority. Additional bathymetric data from gravity surveys were used in the preparation of the bathymetric grid.

**LEGEND**



**SEISMIC INTERPRETATION**  
Bjølset et al. in press

Fault

Målestokk, Scale 1 : 500 000

Detatt: 2000  
Map projection: UTM, Zone 32N, Datum: WGS 84, Spheroid: WGS 84

**NORDLAND AEROMAGNETIC SURVEY 1994**  
FLIGHT LINES - BATHYMETRY AND TOPOGRAPHY  
Norwegian Mapping Authority  
NGU Report 95.040 Map 9, Scale 1 : 500 000

Fig. 15. Flight lines, bathymetry and topography. (Map 9 at a reduced scale.)

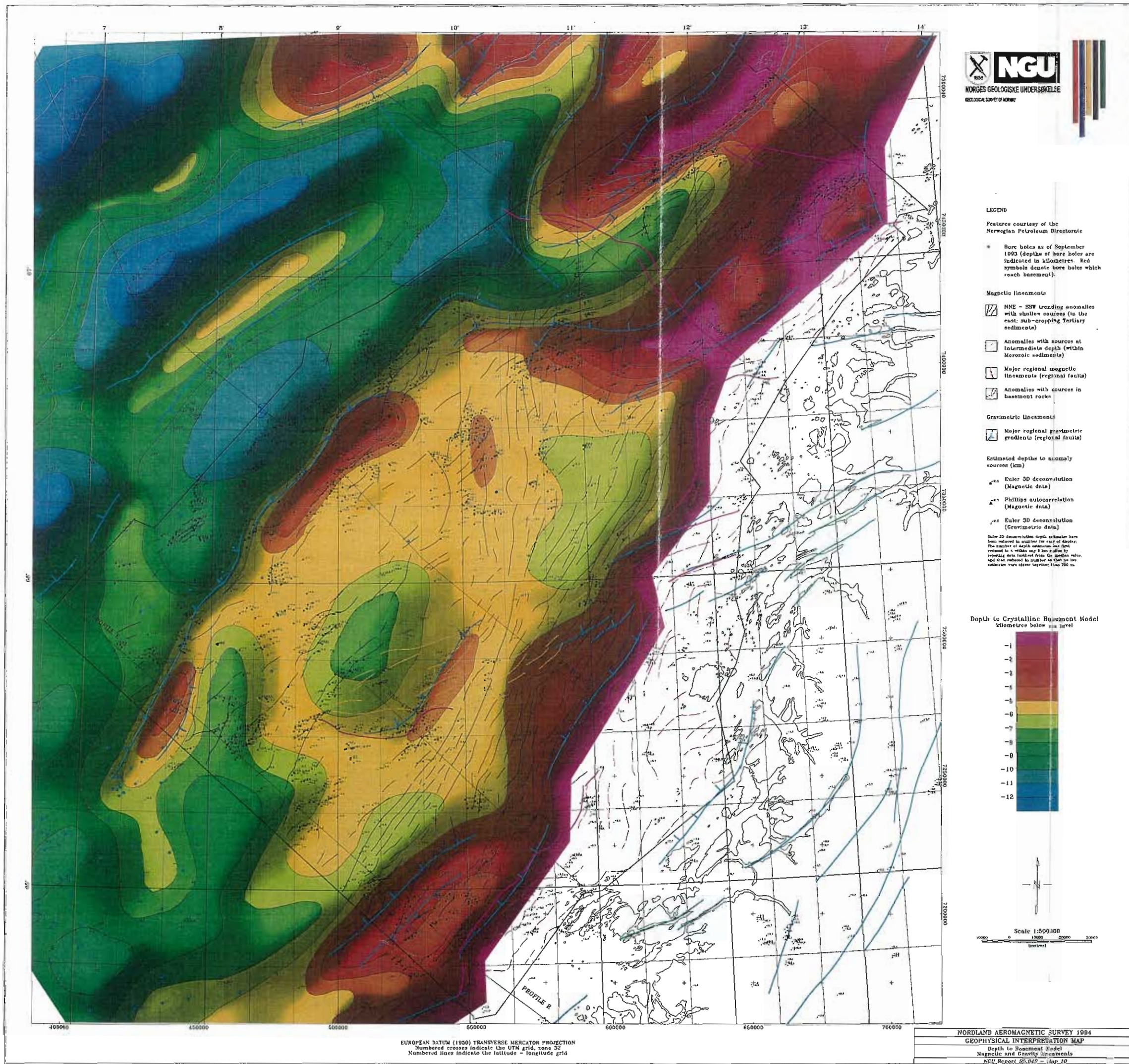


Fig. 16. Geophysical interpretation map. (Map 10 at a reduced scale.)

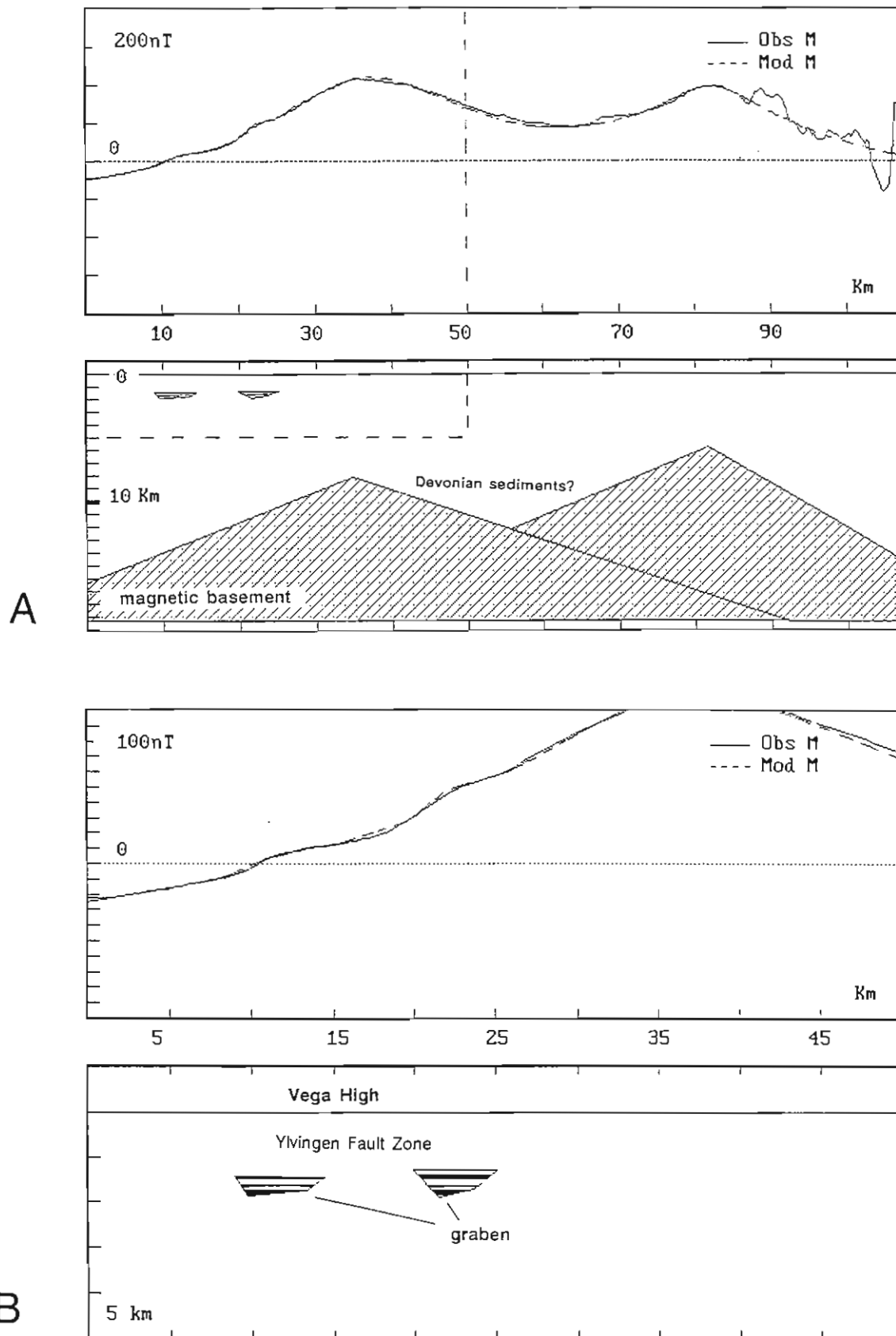


Fig. 17. A) Magnetic modelling of the eastern part of Profile NAS-410 traversing the Vega High. The magnetic anomalies coincide with the graben segments within the Ylvingen Fault Zone. B) is an enlargement of part of (A) shown by the dashed lines. The shape of the early Cretaceous graben infill is taken from seismic profile MN88-407. A susceptibility contrast of  $200 \times 10^5$  SI (and a  $Q$ -value of 0.5) must be used to produce the observed anomaly. This is, however, higher than the measured susceptibility contrast between Jurassic sandstones and Lower Cretaceous silt- and clay-stones from the cores at IKU (maximum  $100 \times 10^5$  SI). Lateral variations in susceptibility within the various units may explain the discrepancy.

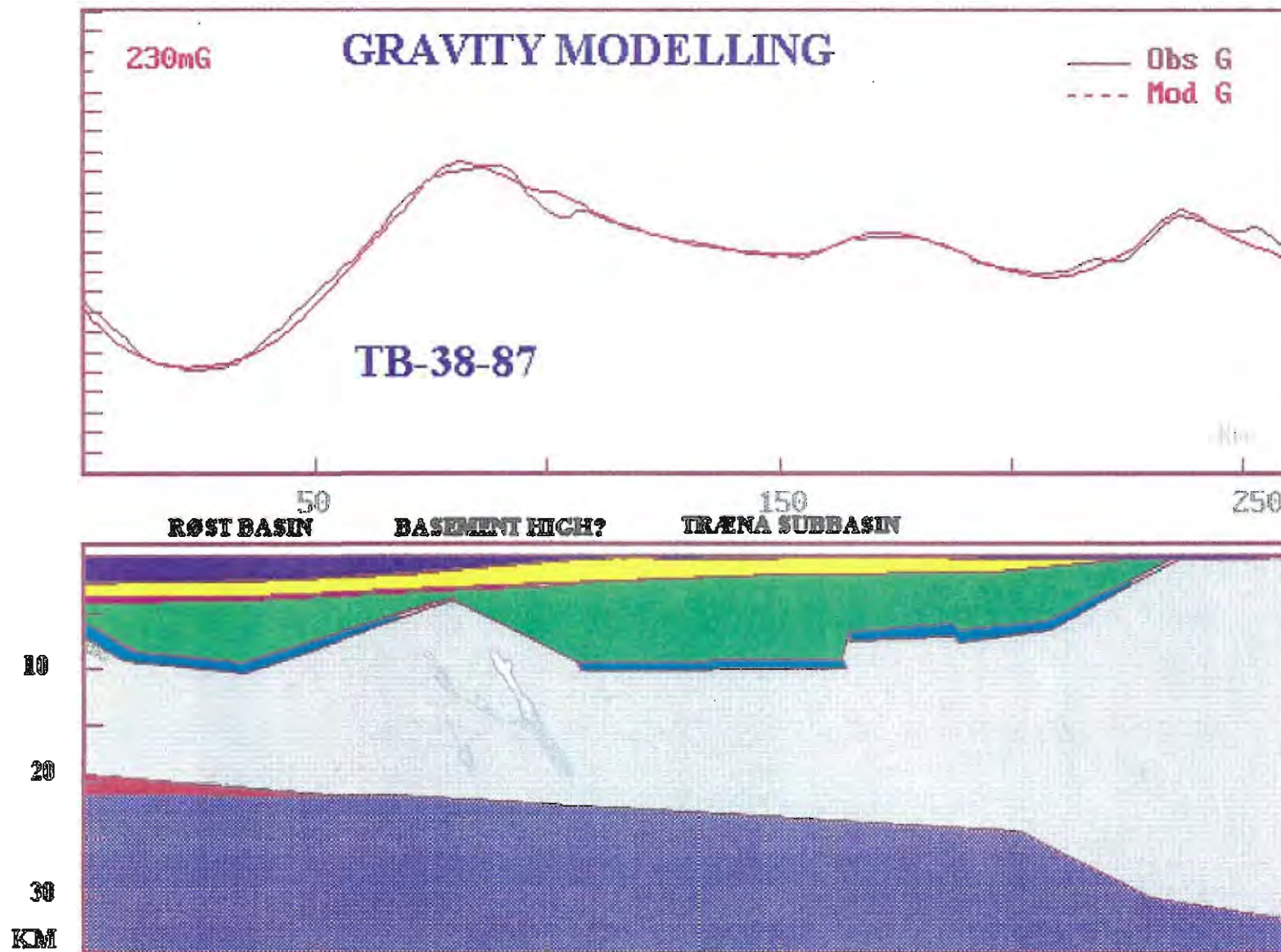


Fig. 18a. Gravity interpretation along seismic profile TB-38-87 (Olesen et al. 1993) to a depth of 35 km. The densities used are shown in Table 2. The location of the profile is indicated on Maps 5-8 & 10 and Figs. 11-14 & 16.

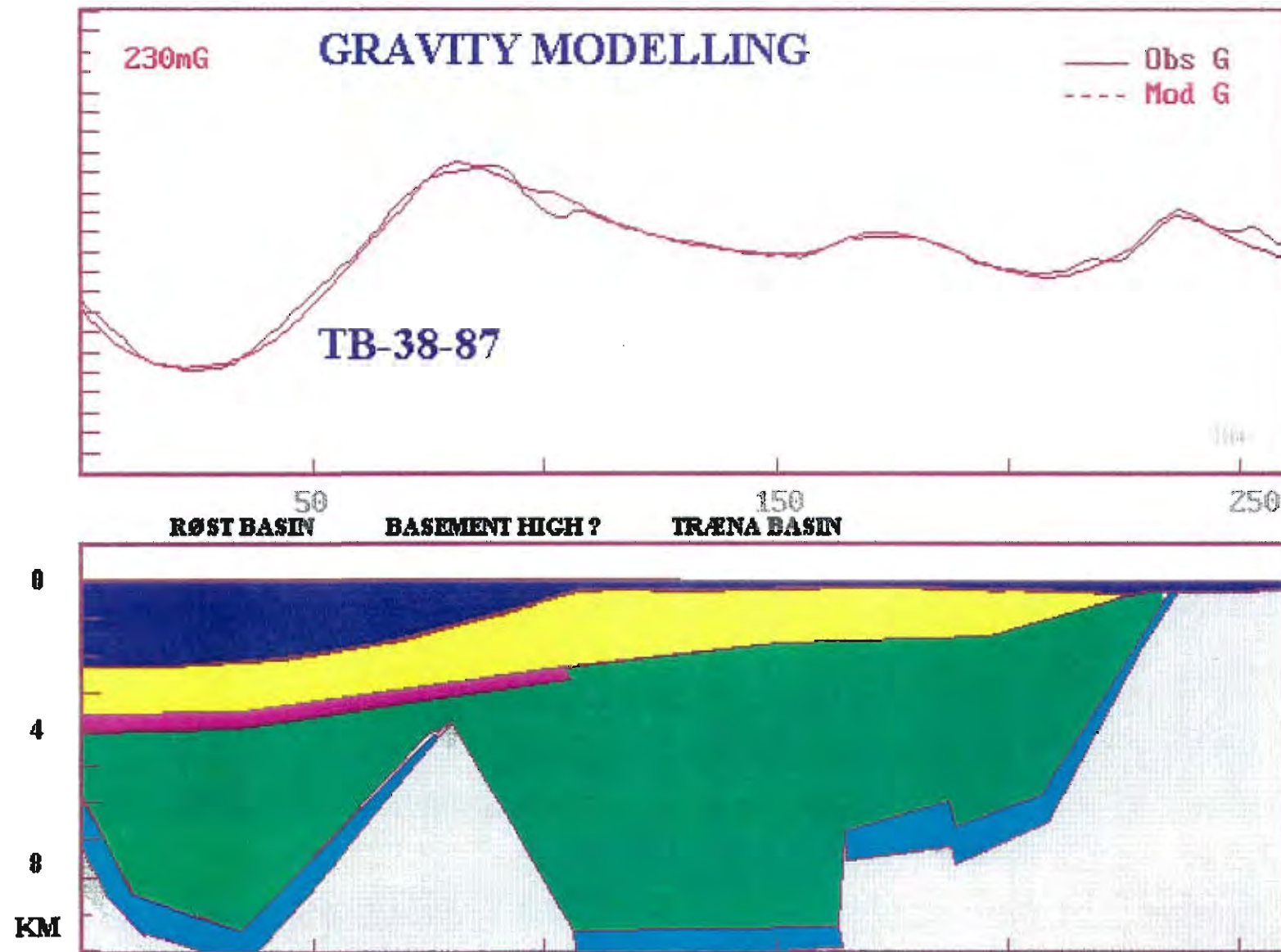


Fig. 18b As Fig. 18a but to a depth of 10 km.

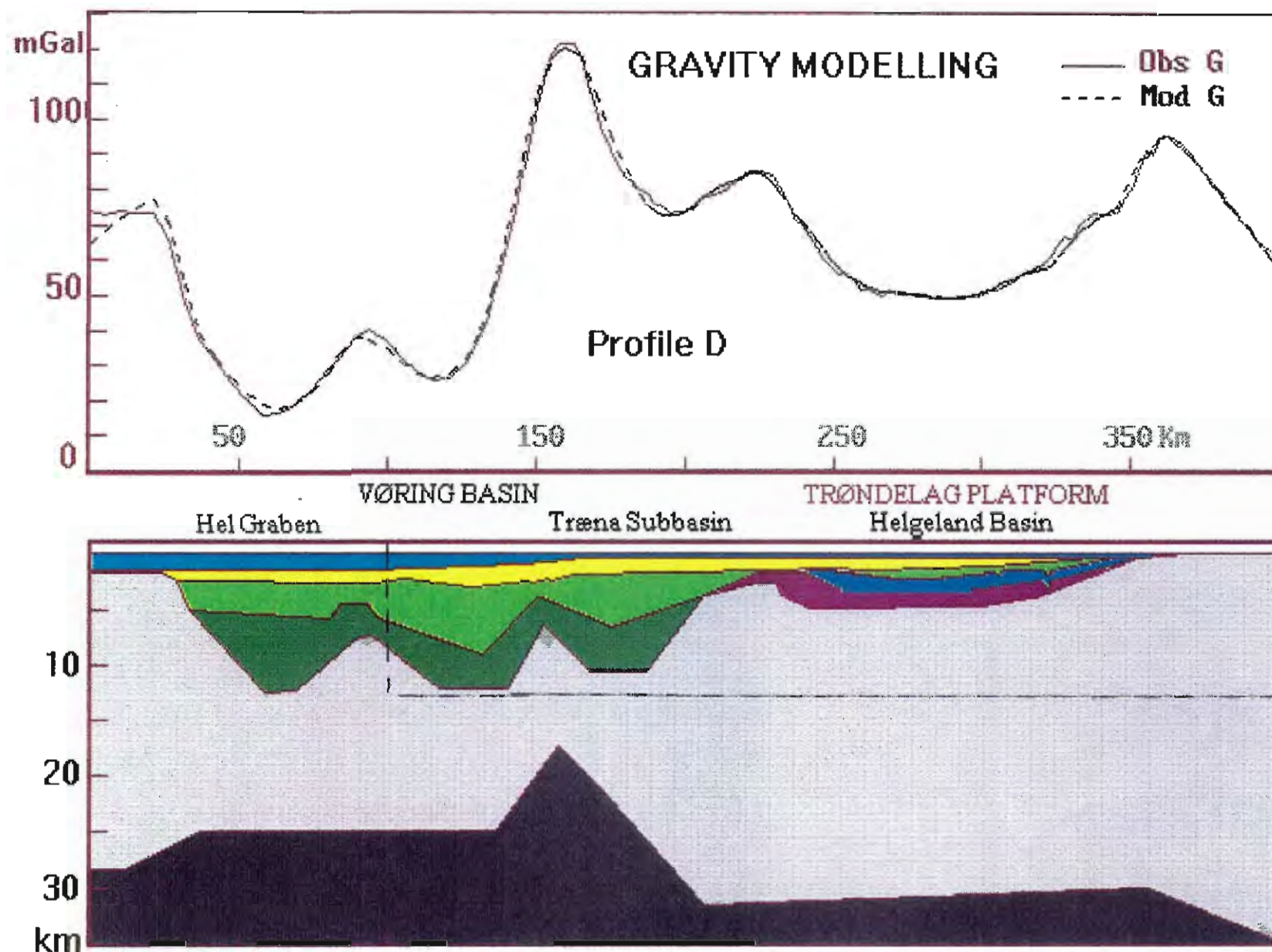


Fig. 19a. Gravity interpretation along seismic profile D (Blystad et al. in press.) to a depth of 35 km. The seismic interpretation from Blystad et al. (in press.) was digitised and depth-converted using the seismic velocities in Table 3. The applied densities are shown in Table 2. The location of the profile is shown on Maps 7 & 10, and Figs. 11-14 & 16. The most detailed interpretation is carried within the NAS-94 area (the Nordland Ridge and the Trøndelag Platform) while the interpretation in the Vøring Basin is more general.

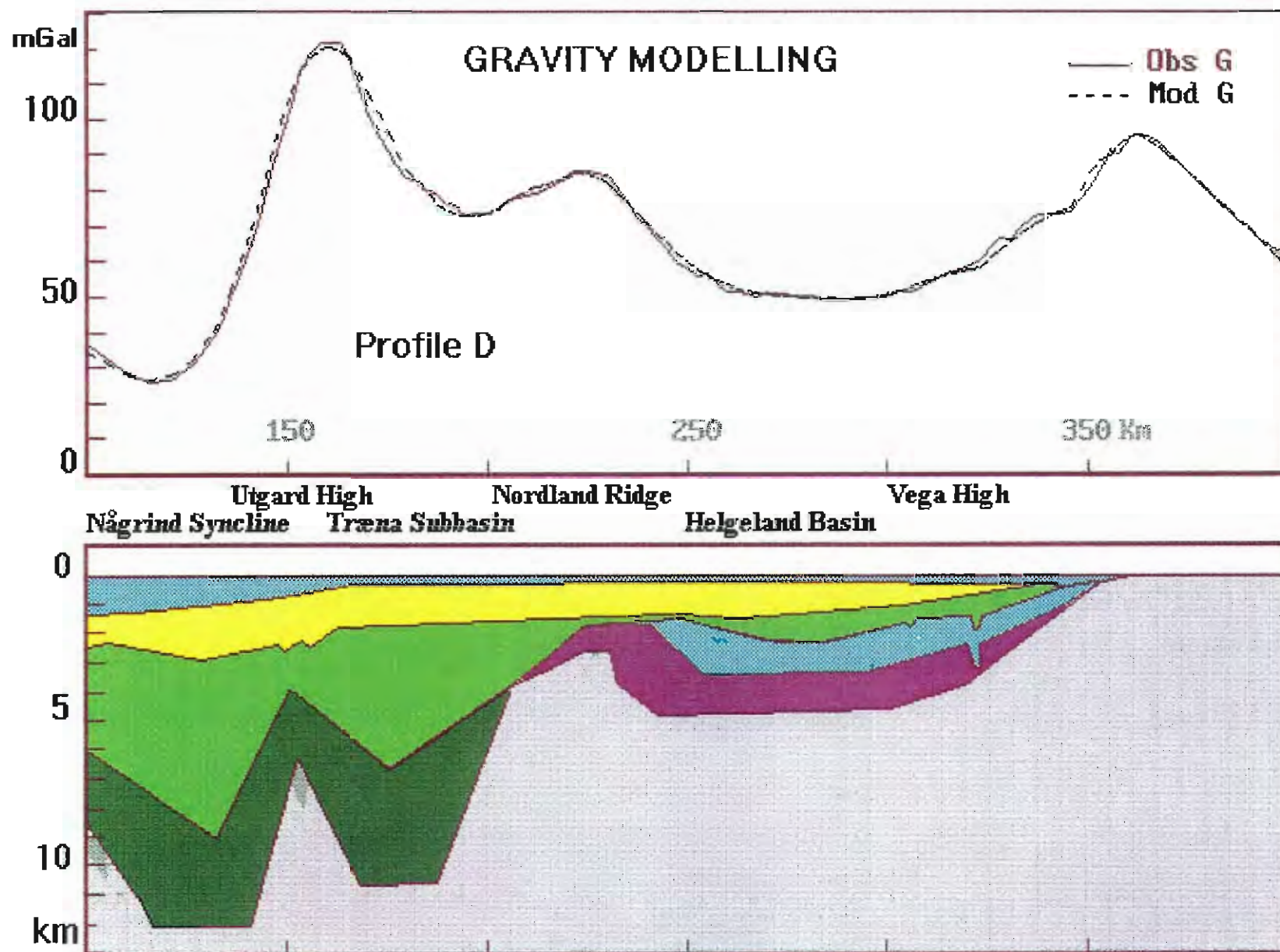


Fig. 19b. An enlargement of part of Fig. 19a shown by the dashed lines, interpreted to a depth of 13 km.



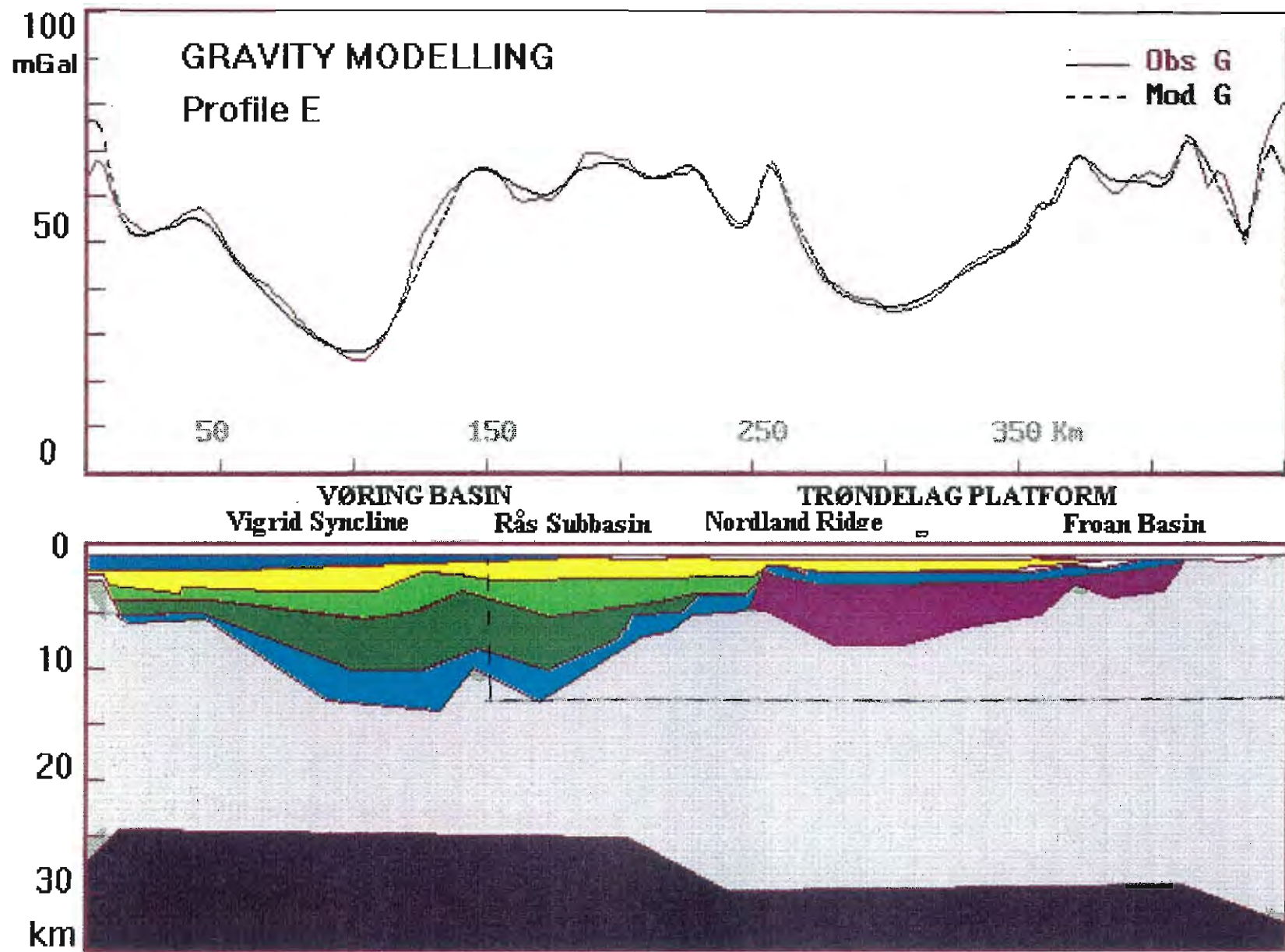


Fig. 20a. Gravity interpretation along seismic profile E (Blystad et al. in press.) to a depth of 35 km. The seismic interpretation from Blystad et al. (in press.) was digitised and depth-converted using the seismic velocities in Table 3. The applied densities are shown in Table 2. The location of the profile is shown on Maps 5-8 & 10, and Figs. 11-14 & 16. The most detailed interpretation is carried within the NAS-94 area (the Nordland Ridge and the Trøndelag Platform) while the interpretation in the Vøring Basin is more general.

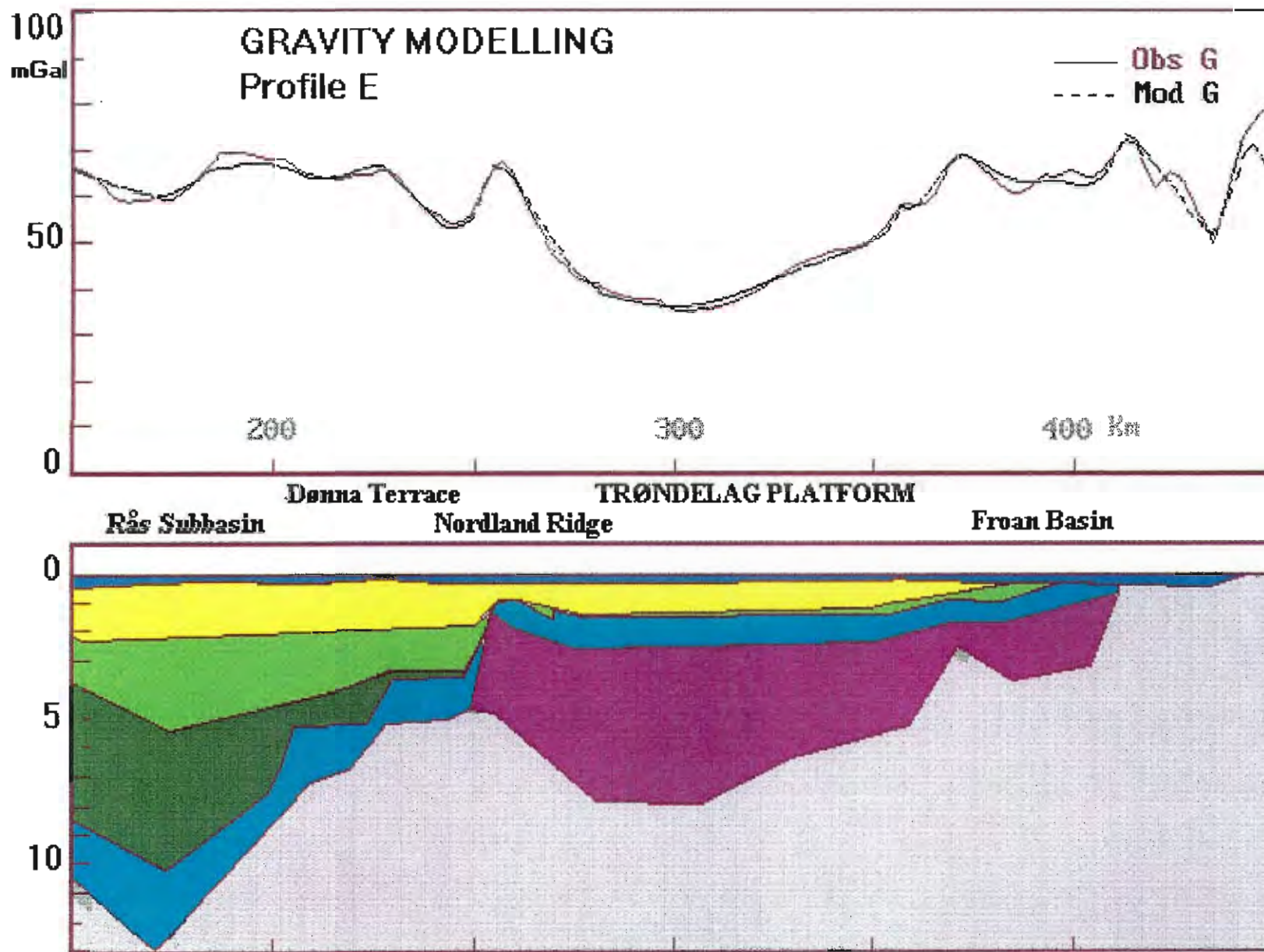


Fig. 20b. An enlargement of part of Fig. 20a shown by the dashed lines, interpreted to a depth of 13 km.



**LEGEND**

Features courtesy of the Norwegian Petroleum Directorate

Jurassic/Early Cretaceous faults

Bore holes as of September 1993

Shaded relief effect  
'illumination' from the southeast  
Shading of shorter wavelength features only

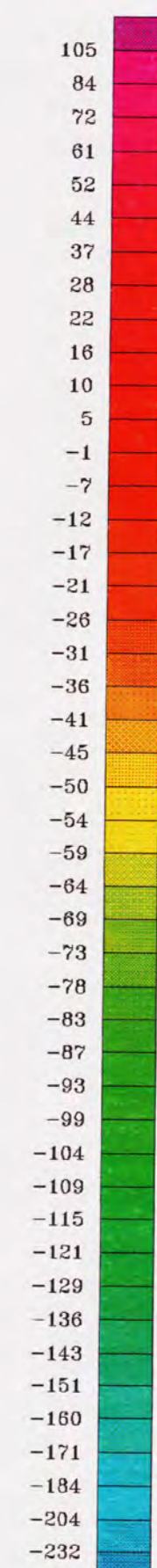
Estimated depths to anomaly sources (km)

2.5 Euler 3D deconvolution (Magnetic data)

2.5 Phillips autocorrelation (Magnetic data)

2.5 Euler 3D deconvolution (Gravimetric data)

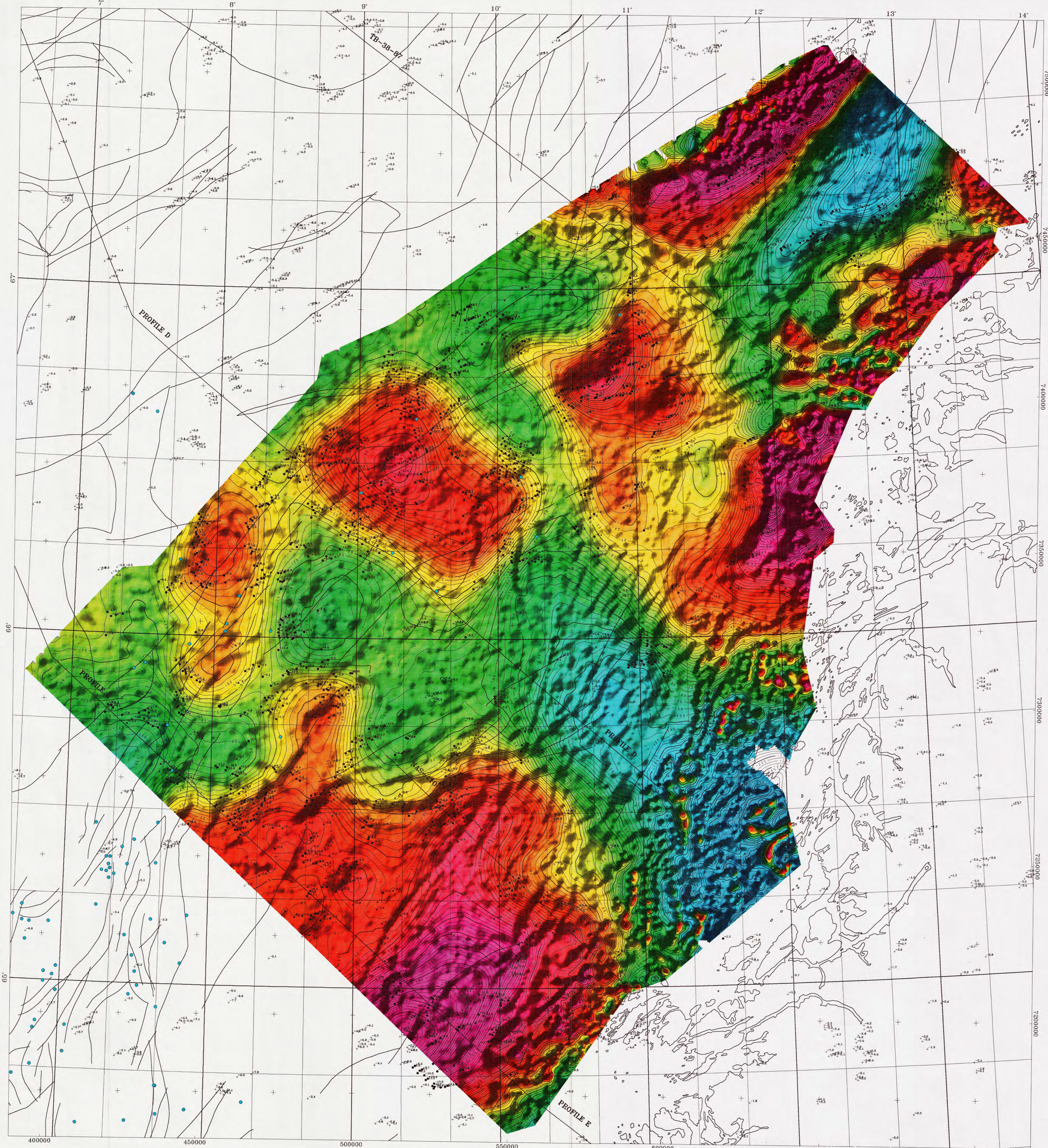
Euler 3D deconvolution depth estimates have been reduced in number for ease of display. The number of depth estimates was first reduced to 4 within any 2 km radius by rejecting data furthest from the median value, and then reduced in number so that no two estimates were closer together than 700 m.



nano-Tesla



Scale 1:500000  
0 10000 20000 30000  
(metres)




EUROPEAN DATUM (1950) TRANSVERSE MERCATOR PROJECTION  
Numbered crosses indicate the UTM grid, zone 32  
Numbered lines indicate the latitude - longitude grid


NORDLAND AEROMAGNETIC SURVEY 1994  
TOTAL MAGNETIC FIELD ANOMALY MAP  
Referred to IGRF 1990



**LEGEND**

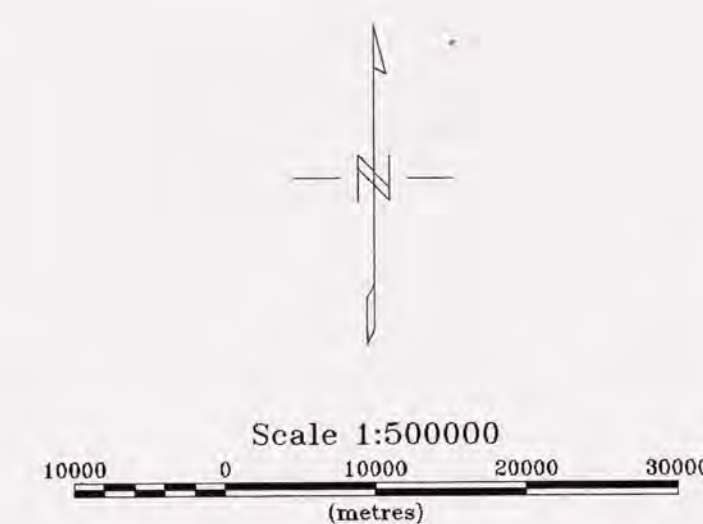
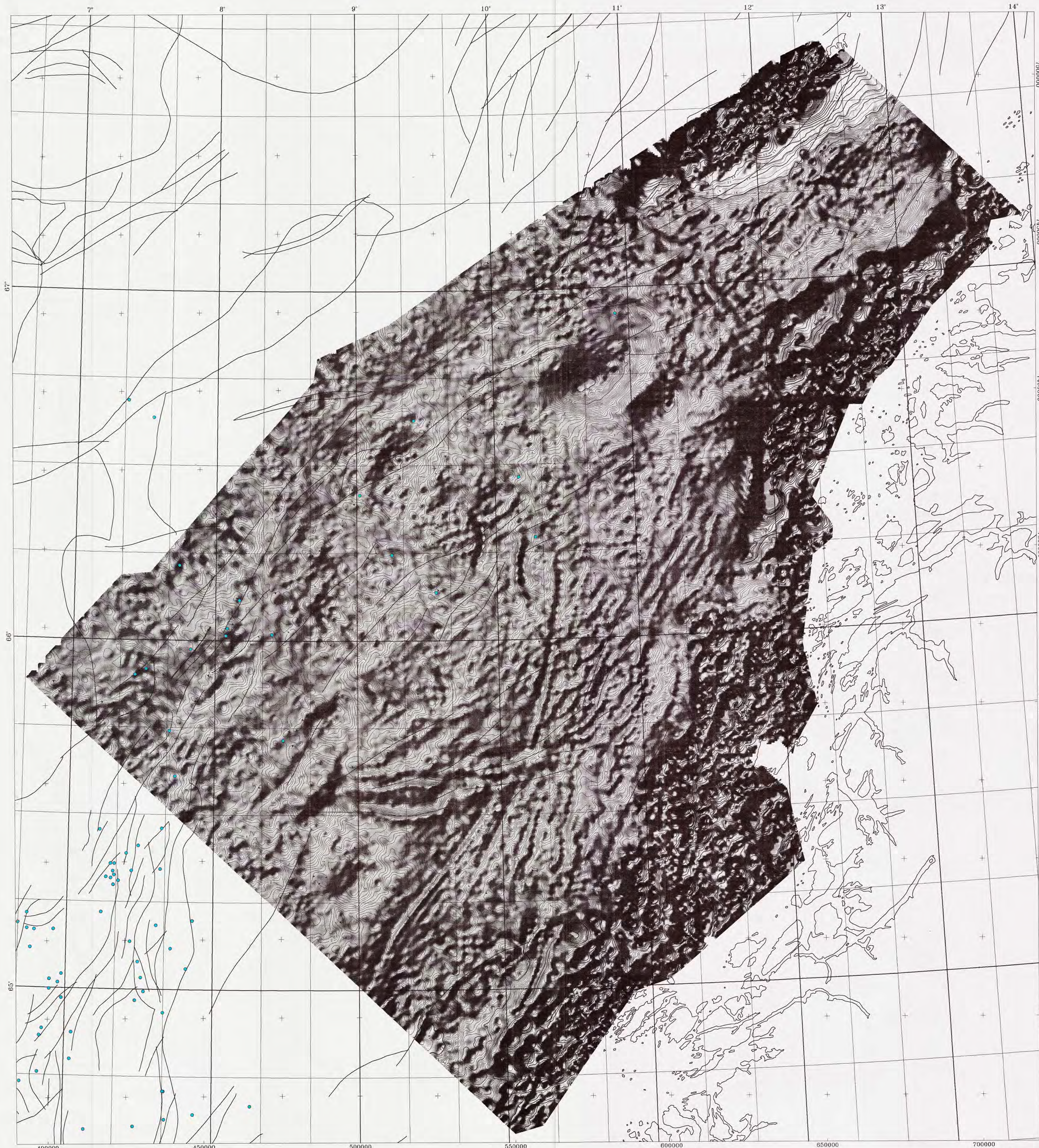
Features courtesy of the Norwegian Petroleum Directorate

 Jurassic/Early Cretaceous faults

 Bore holes as of September 1993

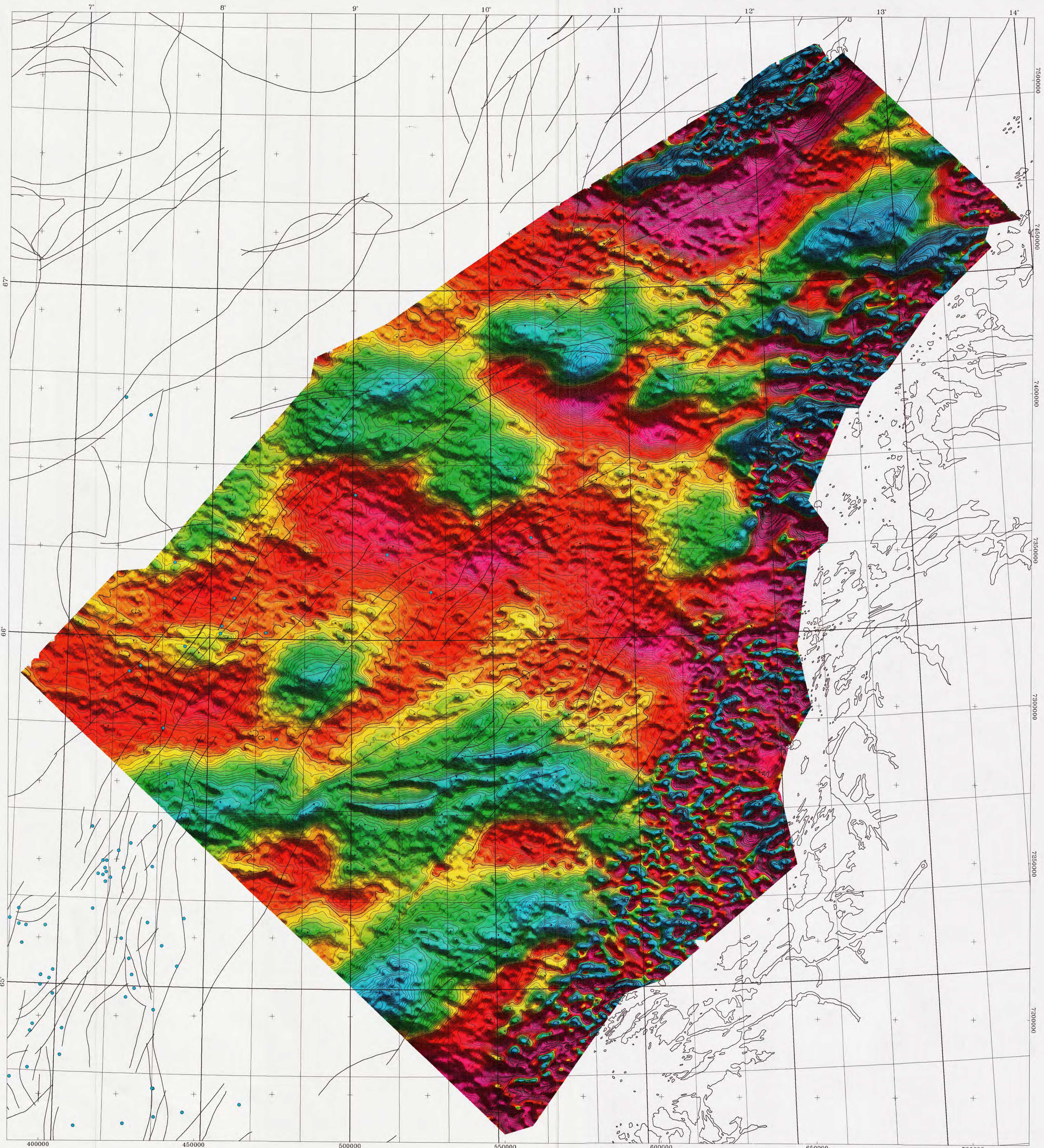
Shaded relief effect 'Illumination' from the southeast

Contour units pico-Tesla per metre



EUROPEAN DATUM (1950) TRANSVERSE MERCATOR PROJECTION  
 Numbered crosses indicate the UTM grid, zone 32  
 Numbered lines indicate the latitude - longitude grid

NORDLAND AEROMAGNETIC SURVEY 1994  
 MAGNETIC GRADIENT AMPLITUDE MAP (ANALYTICAL SIGNAL)  
 Grey-tone presentation  
 NGU Report 95.040 - Map 2

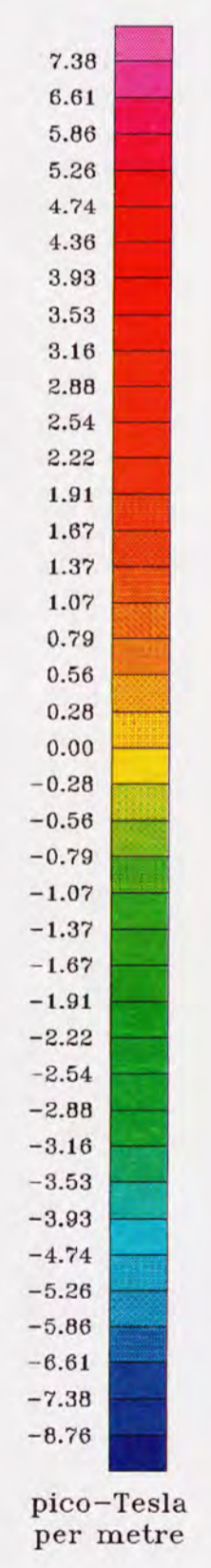


**LEGEND**

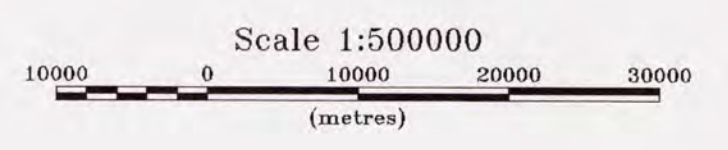
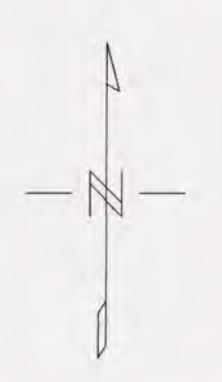
Features courtesy of the Norwegian Petroleum Directorate

- Jurassic/Early Cretaceous faults
- Bore holes as of September 1993

Shaded relief effect 'Illumination' from the south-southwest



pico-Tesla per metre



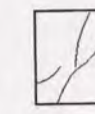
EUROPEAN DATUM (1950) TRANSVERSE MERCATOR PROJECTION  
 Numbered crosses indicate the UTM grid, zone 32  
 Numbered lines indicate the latitude - longitude grid


**NORDLAND AEROMAGNETIC SURVEY 1994**  
**NORTH-SOUTH HORIZONTAL GRADIENT MAP**  
 Space domain filter  
 NGU Report 95.010 - Map 2



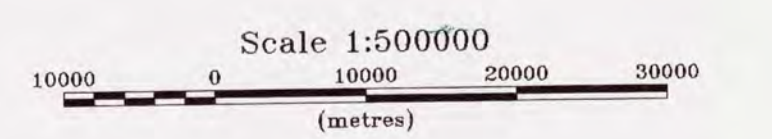
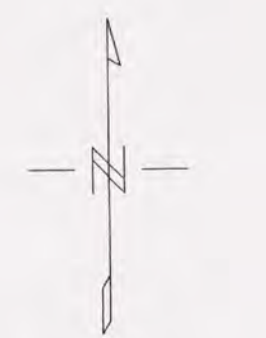
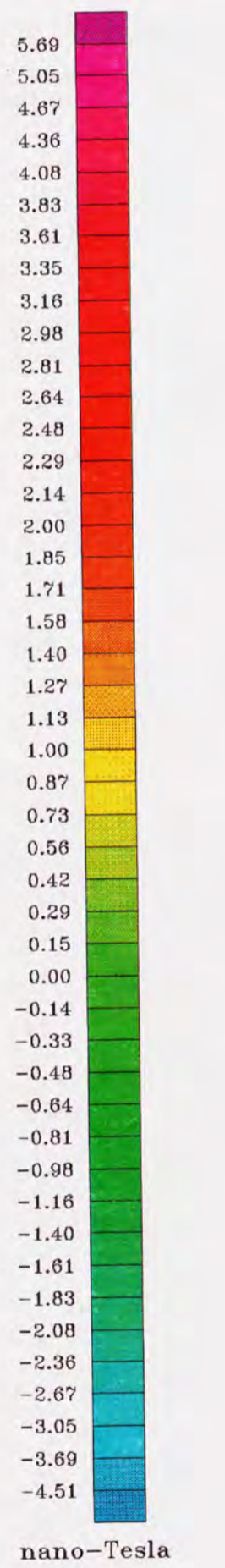
**LEGEND**

Features courtesy of the Norwegian Petroleum Directorate

 Jurassic/Early Cretaceous faults

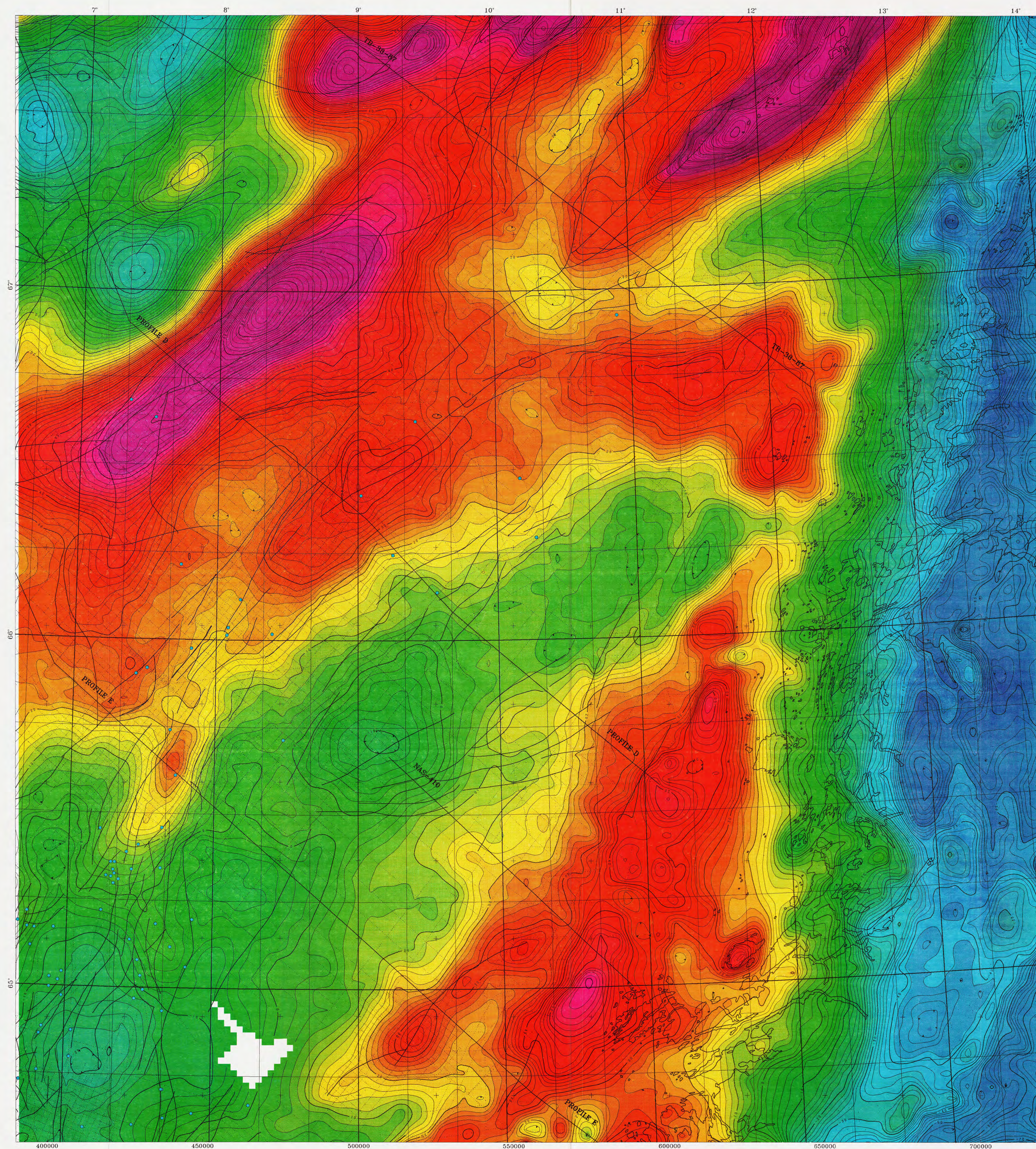
 Bore holes as of September 1993

Shaded relief effect  
'Illumination' from the southeast



EUROPEAN DATUM (1950) TRANSVERSE MERCATOR PROJECTION  
 Numbered crosses indicate the UTM grid, zone 32  
 Numbered lines indicate the latitude - longitude grid

**NORDLAND AEROMAGNETIC SURVEY 1994**  
**RESIDUAL MAGNETIC ANOMALY MAP**  
 Frequency domain filter: 15 km Gaussian residual  
 NGU Report 95.040 - Map 4

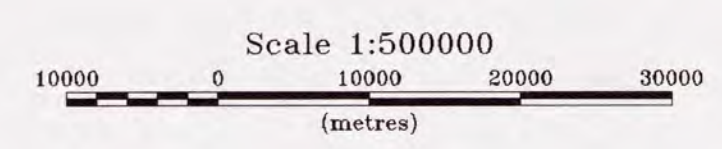
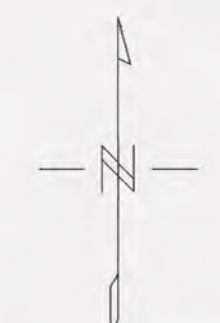
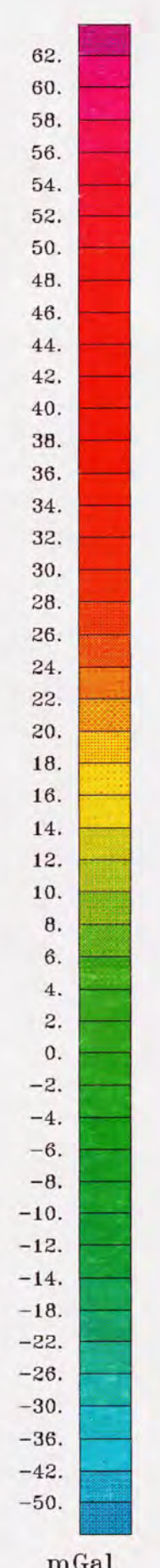


**LEGEND**

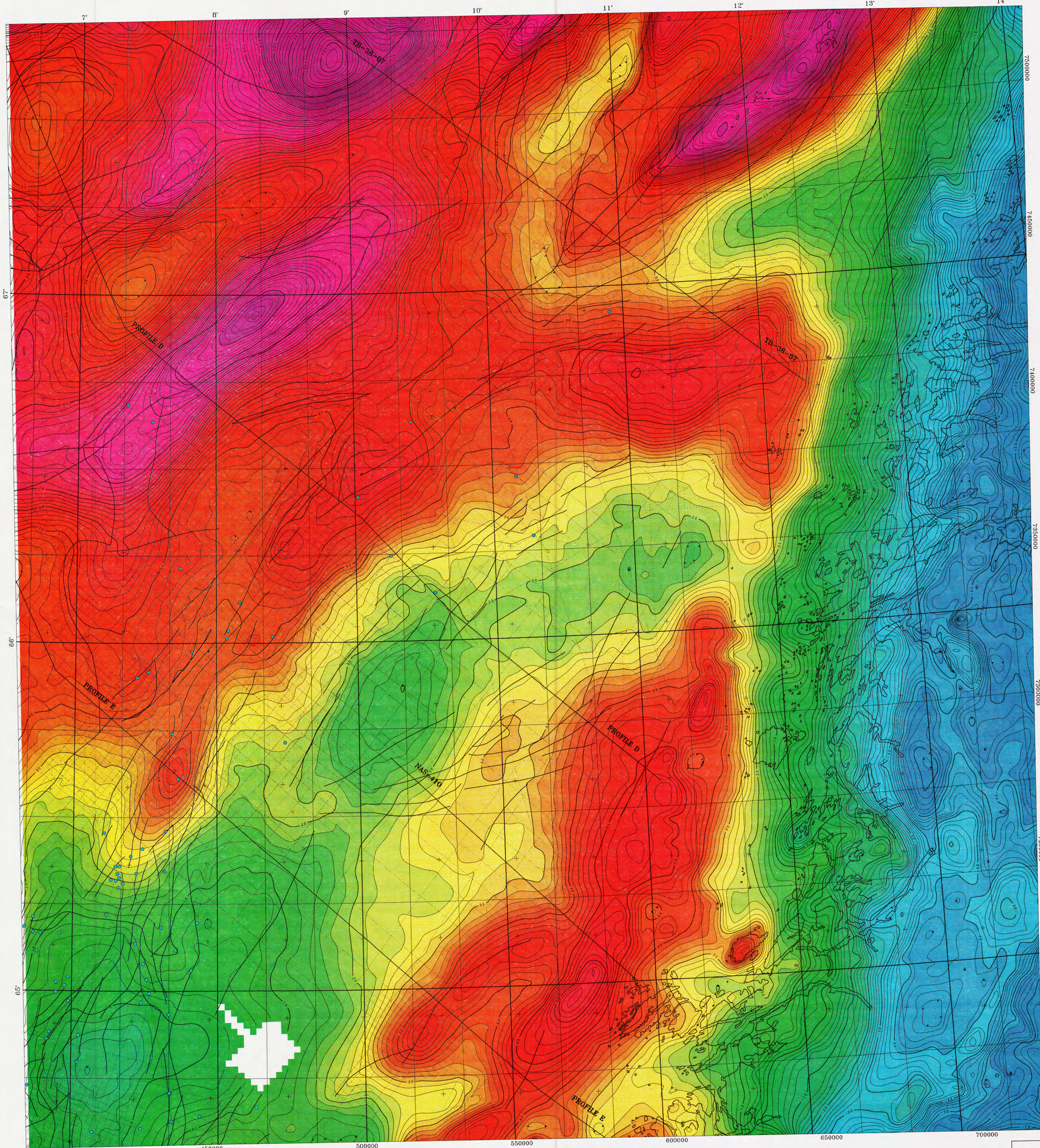
Features courtesy of the Norwegian Petroleum Directorate

Jurassic/Early Cretaceous faults

Bore holes as of September 1993



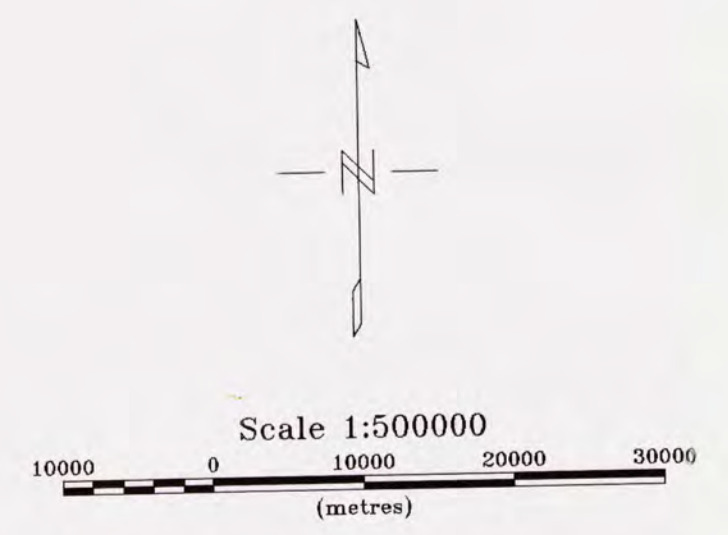
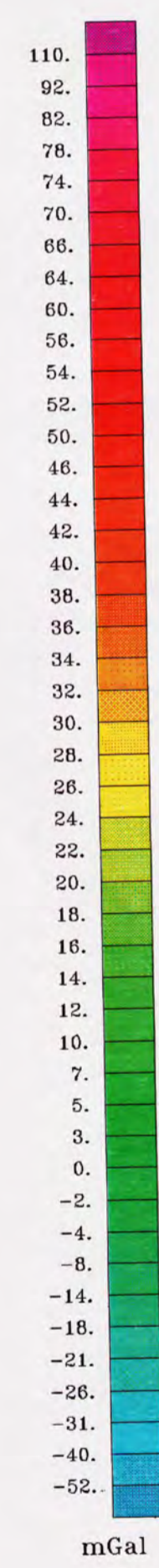
EUROPEAN DATUM (1950) TRANSVERSE MERCATOR PROJECTION  
Numbered crosses indicate the UTM grid, zone 32  
Numbered lines indicate the latitude - longitude grid



**LEGEND**

Features courtesy of the Norwegian Petroleum Directorate

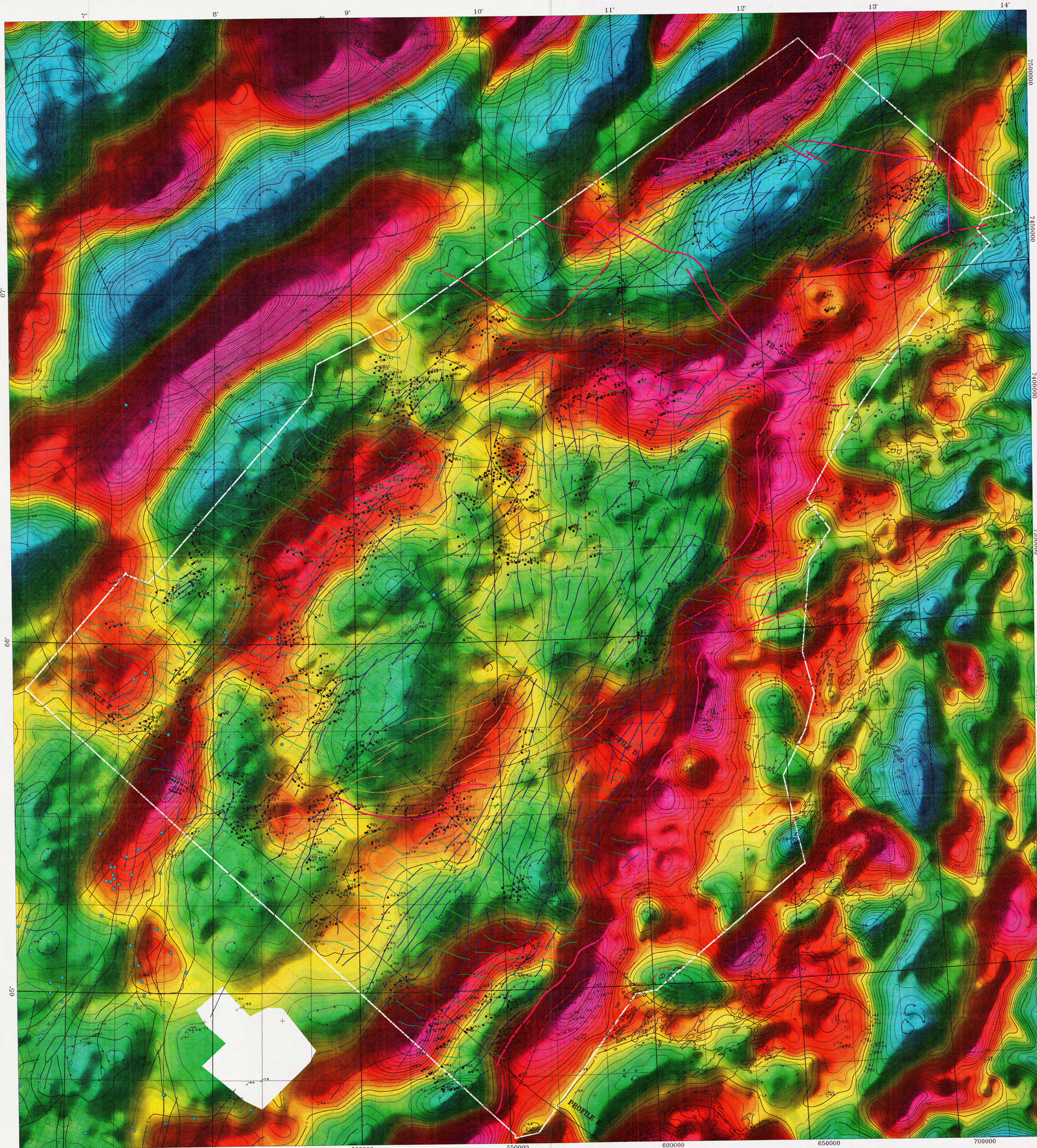
- Jurassic/Early Cretaceous faults
- Bore holes as of September 1993



EUROPEAN DATUM (1950) TRANSVERSE MERCATOR PROJECTION  
 Numbered crosses indicate the UTM grid, zone 32  
 Numbered lines indicate the latitude - longitude grid

NAS-94 PROJECT  
 BOUGUER GRAVITY ANOMALY MAP  
 Referred to IGSN 71  
 NGU Report 95.040 - Map 6





**LEGEND**

Features courtesy of the Norwegian Petroleum Directorate

- Jurassic/Early Cretaceous faults
- Bore holes as of September 1993

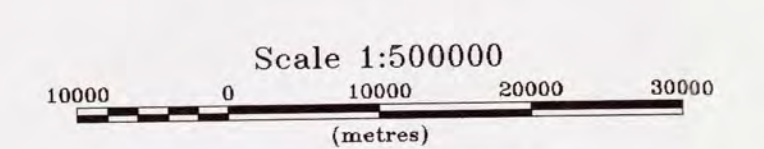
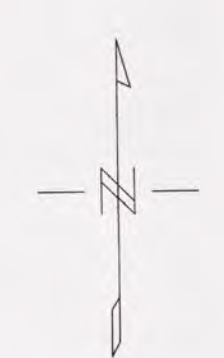
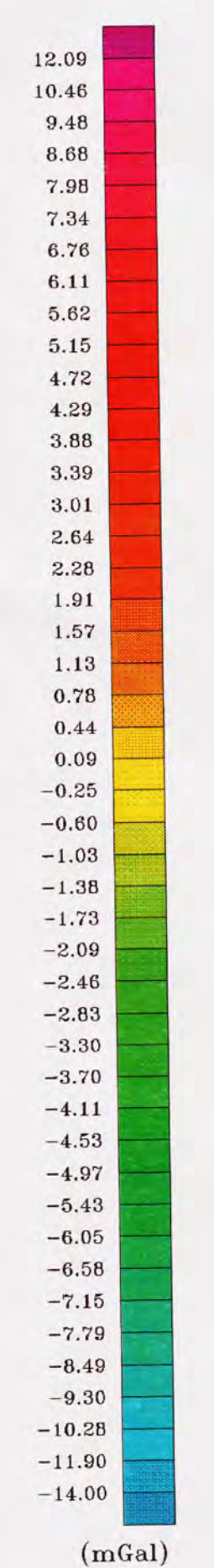
**Magnetic lineaments**

- Area of high frequency irregular anomalies (Intrusives/extrusives ?)
  - NW - ESE trending anomalies with shallow sources (Quaternary overburden ?)
  - NNE - SSW trending anomalies with shallow sources (In the east: sub-cropping Tertiary sediments ?)
  - Anomalies with sources at intermediate depth (Sources within Mesozoic sediments)
  - Major regional magnetic lineaments (Regional faults)
  - Anomalies with sources in basement rocks
- Broken lines denote diffuse features

**Estimated depths to anomaly sources (km)**

- Euler 3D deconvolution (Magnetic data)
- Phillips autocorrelation (Magnetic data)
- Euler 3D deconvolution (Gravimetric data)

Euler 3D deconvolution depth estimates have been reduced in number for ease of display; The number of depth estimates was first reduced to 4 within any 2 km radius by rejecting data furthest from the median value, and then reduced in number so that no two estimates were closer together than 700 m.





**NORDLAND AEROMAGNETIC SURVEY 1994**  
**RESIDUAL BOUGUER GRAVITY ANOMALY MAP**  
 100 km Gaussian residual filter  
 Magnetic lineaments from Map 94.074-09 superimposed  
 NGU Report 95.040 - Map 07

EUROPEAN DATUM (1950) TRANSVERSE MERCATOR PROJECTION  
 Numbered crosses indicate the UTM grid, zone 32  
 Numbered lines indicate the latitude - longitude grid



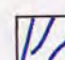


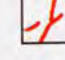


**LEGEND**

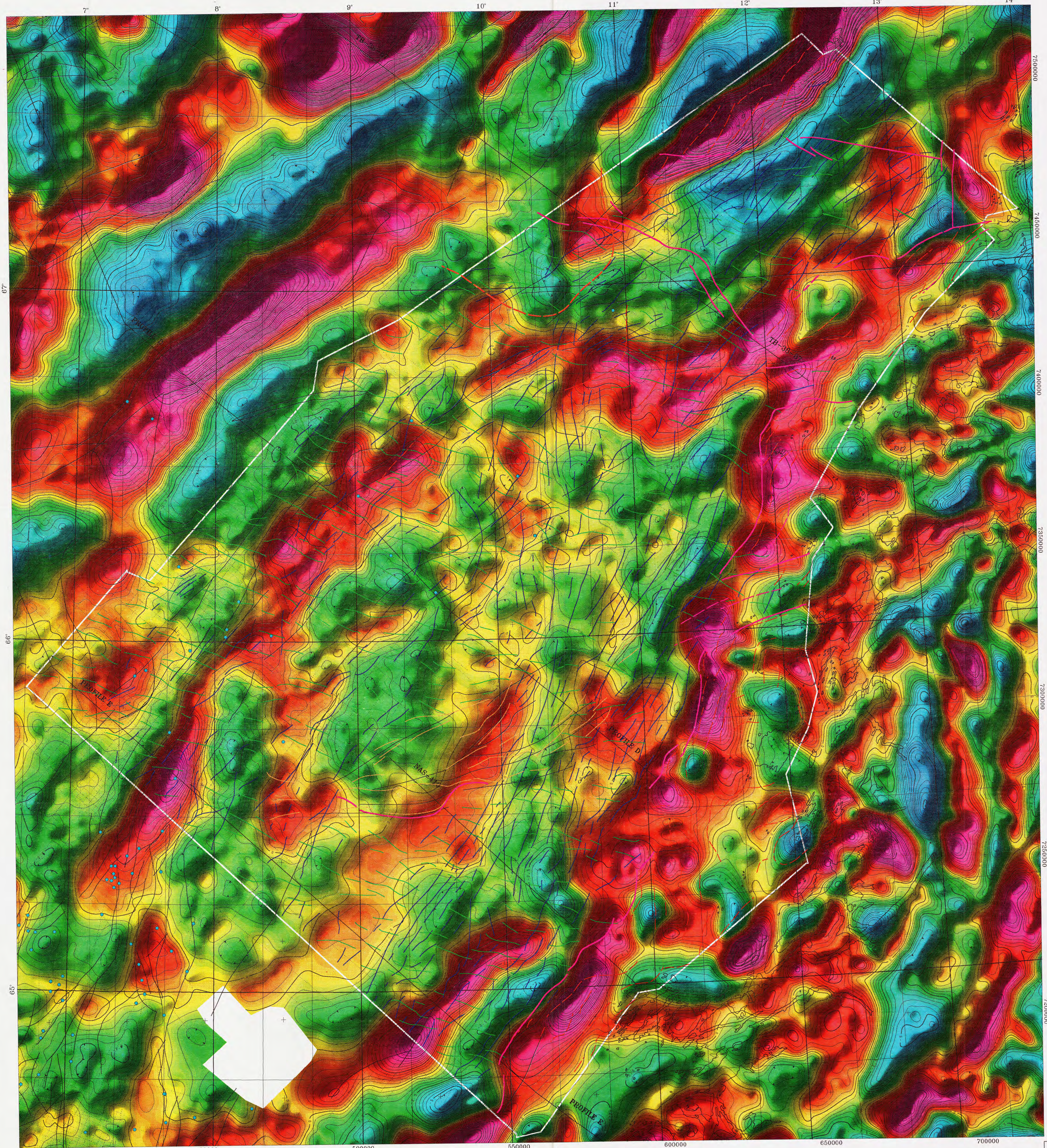
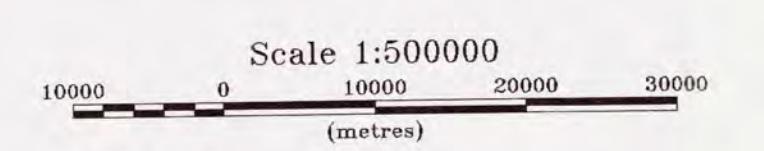
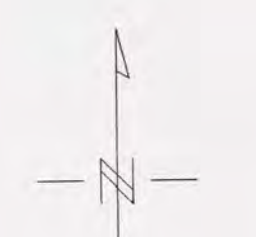
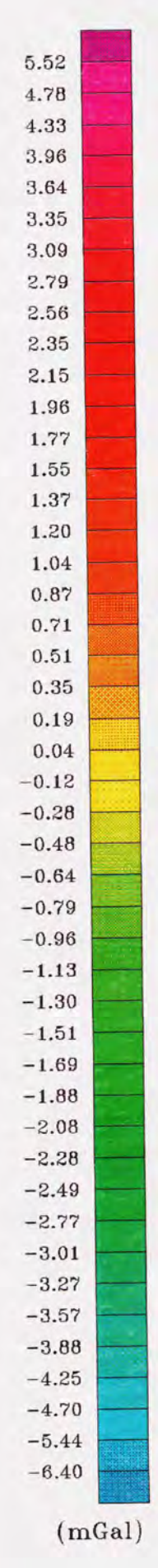
Features courtesy of the Norwegian Petroleum Directorate

-  Jurassic/Early Cretaceous faults
-  Bore holes as of September 1993

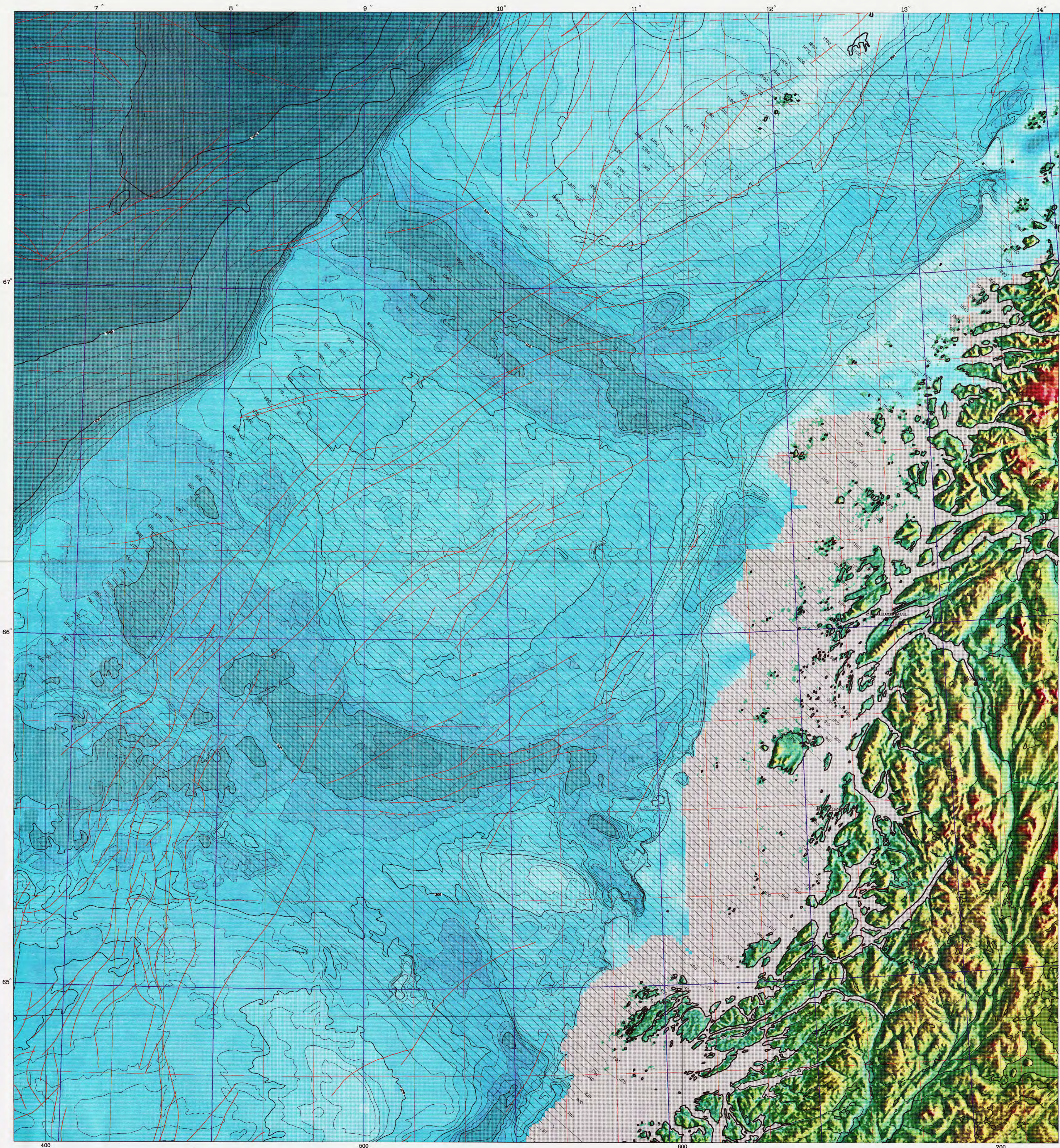
**Magnetic lineaments**

-  Area of high frequency irregular anomalies (Intrusives/extrusives ?)
-  WNW - ESE trending anomalies with shallow sources (Quaternary overburden ?)
-  NNE - SSW trending anomalies with shallow sources (In the east: sub-cropping Tertiary sediments ?)
-  Anomalies with sources at intermediate depth (Sources within Mesozoic sediments)
-  Major regional magnetic lineaments (Regional faults)
-  Anomalies with sources in basement rocks

Broken lines denote diffuse features

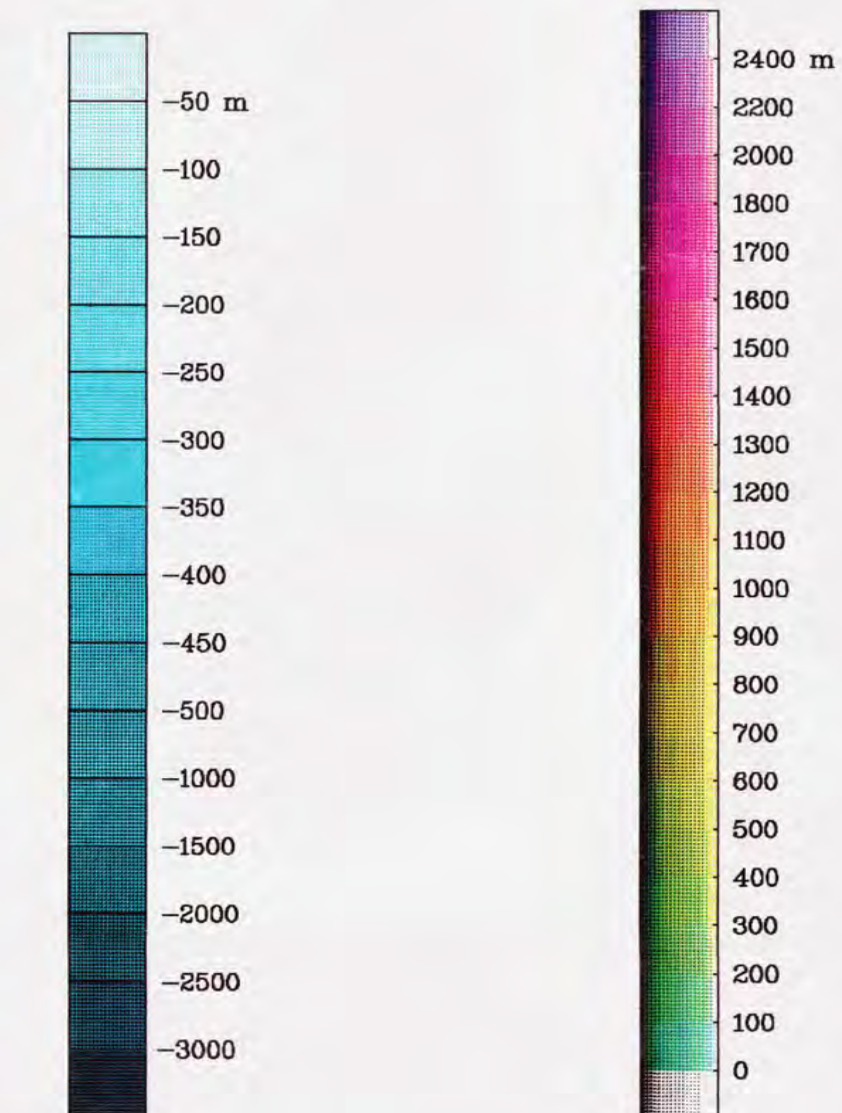


EUROPEAN DATUM (1950) TRANSVERSE MERCATOR PROJECTION  
 Numbered crosses indicate the UTM grid, zone 32  
 Numbered lines indicate the latitude - longitude grid



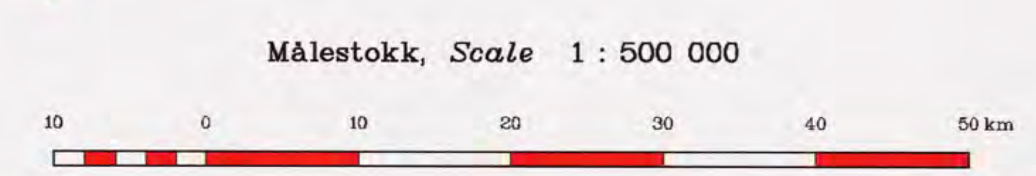
**Map description**  
 The bathymetry is plotted as an ordinary contour map in shades of blue with contour lines every 25 m down to 500 m and every 100 m for greater depths. Thicker lines are used for every 100 m down to 500 m and for every 500 m for greater depths.  
 A pseudo-relief technique with 'illumination' from the east is used for the topography.  
 Data were provided by the Norwegian Mapping Authority. Additional bathymetric data from gravity surveys were used in the preparation of the bathymetric grid.

LEGEND



SEISMIC INTERPRETATION  
 Blystad et al. in press

Fault



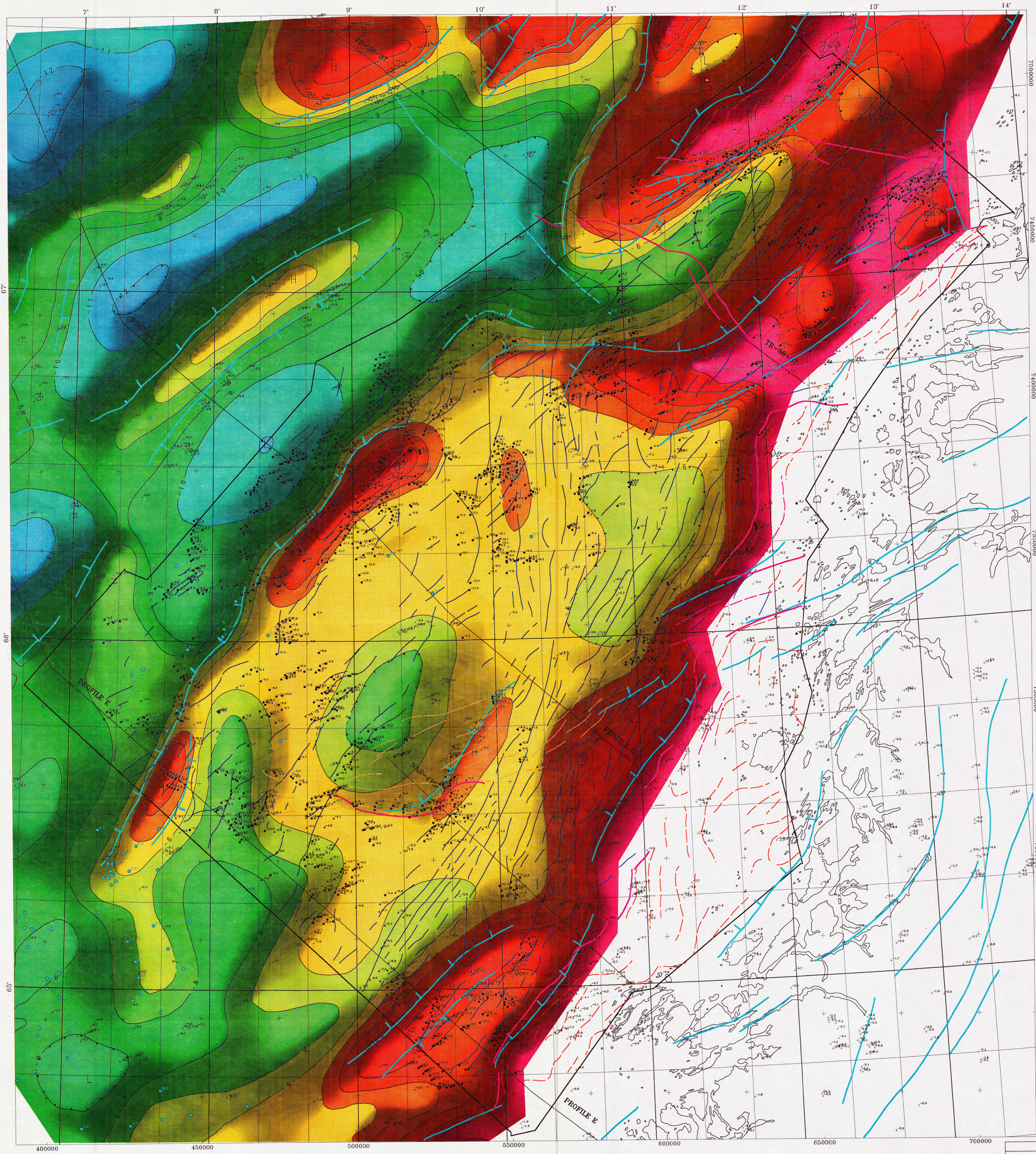
Detour: EDE6  
 Map projection: Universal Transverse Mercator, midmeridian 9° E.Gr.

NORDLAND AEROMAGNETIC SURVEY 1994

FLIGHT LINES - BATHYMETRY AND TOPOGRAPHY

Norwegian Mapping Authority

NGU Report 95.040 MAP 09, Scale 1 : 500 000



**LEGEND**

Features courtesy of the Norwegian Petroleum Directorate

- Bore holes as of September 1993 (depths of bore holes are indicated in kilometres. Red symbols denote bore holes which reach basement).

**Magnetic lineaments**

- NNE - SSW trending anomalies with shallow sources (in the east: sub-cropping Tertiary sediments)
- Anomalies with sources at intermediate depth (within Mesozoic sediments)
- Major regional magnetic lineaments (regional faults)
- Anomalies with sources in basement rocks

**Gravimetric lineaments**

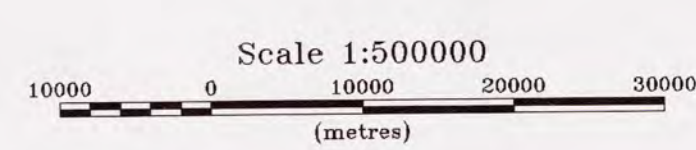
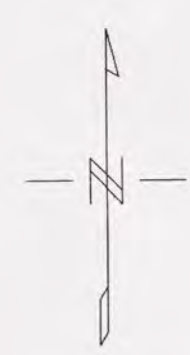
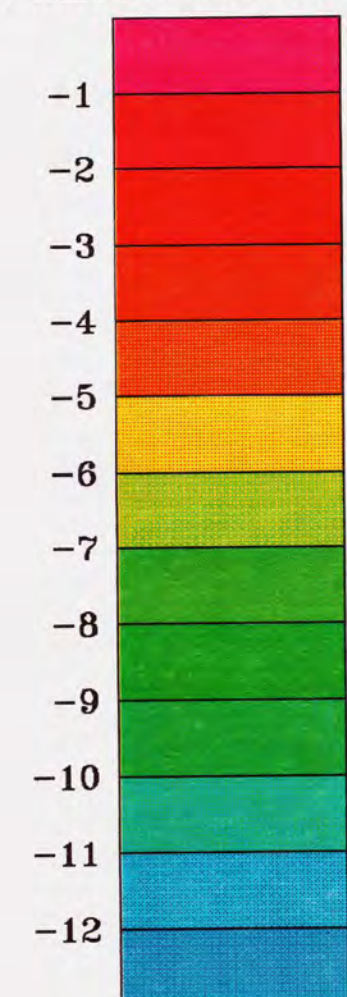
- Major regional gravimetric gradients (regional faults)

**Estimated depths to anomaly sources (km)**

- Euler 3D deconvolution (Magnetic data)
- ▲ Phillips autocorrelation (Magnetic data)
- Euler 3D deconvolution (Gravimetric data)

Euler 3D deconvolution depth estimates have been reduced in number for ease of display. The number of depth estimates was first reduced to 4 within any 2 km radius by rejecting data furthest from the median value, and then reduced in number so that no two estimates were closer together than 700 m.

**Depth to Crystalline Basement Model**  
kilometres below sea level



EUROPEAN DATUM (1950) TRANSVERSE MERCATOR PROJECTION  
Numbered crosses indicate the UTM grid, zone 32  
Numbered lines indicate the latitude - longitude grid